NTNU

Norwegian University of
Science and Technology

Partial Discharges on an Epoxy Surface due to Water Droplets

Bernt Milne Grieg

Master of Science in Physics and Mathematics

Submission date: June 2011

Supervisor: Steinar Raaen, IFY

Co-supervisor: Sverre Hvidsten, SINTEF energiforskning AS
Frank Mauseth, ELKRAFT
Pål Keim Olsen, SmartMotor AS

Norwegian University of Science and Technology
Department of Physics

Partial Discharges on an Epoxy Surface due to Water Droplets

Bernt M. Grieg
Faculty of Natural Science and Technology
Department of Physics, NTNU, Trondheim, Norway

June 30, 2011

Abstract

Offshore wind turbines are exposed to a very harsh environment and can sustain significant damage during operation. In this thesis work, the possibilities of partial discharges in an insulation system of an offshore wind turbine were investigated. The insulation system that was studied was a hybrid system. The system was made up of an epoxy filler and a shell made out of glass fiber enforced epoxy composite. In addition to these two epoxy components there was an oil component. It was this oil that was the main focus of this thesis. It was theorized that if the oil was allowed to diffuse into the glass fiber enforced epoxy composite surface it would change the aging situation. The validity of this theory was investigated with a series of experiments and simulations.

The experiments were done in two parts. The first part was an investigation of the partial discharge situation for the system. The second was an aging test. The experiments were conducted on a test sample, designed to have a similar electrical situation as the turbine. In the partial discharge test water droplets were placed on the surface of the sample and different levels of high voltage were applied. Both deionized and salt water droplets were used. The aging tests were conducted at the voltage levels used in the turbine and at voltage levels were it was known that partial discharges occurred. In the aging test the test samples were periodically exposed to a continuous stream of salt water drops. For 16 h salt water was dripped onto the surface and allowed to flow down the width of it. After the 16 h the sample was left to dry for 8 h. This process was repeated over a period of several days.

When the samples were saturated with oil the voltage level required to create discharges was reduced. In the cases were no oil was present there were no significant discharges recorded around the voltage levels expected in the turbine. For an oil saturated sample discharges were observed at voltage levels around those expected in the turbine. Further investigations are required in order to understand the reasons for these effects.

Preface

This master's thesis work was carried out at the Department of Physics at NTNU and marks the end of a master study in applied physics. The project was done in cooperation with SINTEF Energy AS, SmartMotor AS and NTNU. Two departments from NTNU were represented. I belong to the Department of Physics and since the assignment is closely related to energy aid was given by the Department of Electric Power Engineering.

I would like to thank my advisors for all their help during this project. From SINTEF Energy AS, Dr. Ing. Sverre Hvidsten, from the Department of Electric Power Engineering Associate Professor Frank Mauseth, from SmartMotor AS Pål Keim Olsen and from the Department of Physics Professor Steinar Raaen. Each of them have given me invaluable aid during this semester.

In addition I would like to thank the people at the Natural Science workshop for their help in constructing my lab equipment, Gunnar Berg for his help in interpreting my results, Hans Helmer Sæternes for designing the mold used to create my test sample and SmartMotor AS for supplying me with the materials for my experiments and the opportunity to do this project.

Finally I would like to thank my family for all their support and help during the work on this thesis.

Bernt Milne Grieg

Contents

Chapter 1

Introduction

Today there is a driving force to develop new types of wind turbines and floating towers for deep water deployment offshore. In order to keep a low weight of the turbines, they consist to a large extent of polymeric materials. This also includes the electrical insulation and protecting parts of the design. For some machines, the insulation system is of a hybrid type, with both oil and solid insulation where the oil is being heated by the stator windings. SmartMotor AS has designed a prototype for such a turbine. Since this prototype is still in development details about the design are kept to a minimum and all component names are left out. This thesis work focus only on the properties of the insulation system.

The main purpose of this project was to examine the possible occurrence of surface discharges on the epoxy insulation material during service. For offshore insulation system water is a major concern. Water droplets can increase the chances of surface discharges and lead to more rapid aging of the insulation. The cooling oil could easily diffuse into the surface [1]. The diffusion process and the changes it caused in the permittivity of the insulation was well known. It was not known how this would effect the chances of surface discharges. In order to investigate this a series of experiments and simulations were conducted. In the experiments, water droplets were placed on the insulation surface and exposed to an electric field. The size and conductivity of the droplets were varied. In order to determine what effect the oil had on the situation, the insulation system was saturated with oil and

exposed to the same experiments as a sample without oil. The experimental setup created was based on a design by S. Keim [2]. The test sample used was adjusted in order to accurately replicate the electric field in the wind turbine

In addition to the surface discharge investigations an erosion test was conducted. In the erosion test the sample was exposed to high voltage and salt water for long periods. This was done in order to investigate the possibilities of damages to the system over time. The erosion test was conducted for samples both with and without oil.

1.1 Previous work

Investigation of aging on electric insulators is a very well developed scientific field. The damage caused by water droplet on insulation surfaces has been investigated by many researchers. S. Keim wrote her a PhD thesis on this subject [2]. The experimental setup used in this thesis work was based on her design. M. G. Danikas investigated how the conductivity of the droplets affected the behavior of the droplets in electric fields. A. Moukengué Imano conducted detailed simulations on how sessile water droplets enhanced an electric field on the surface of an insulator.

Chapter 2

Theory

2.1 Water properties

There are many different types of water, rain water, sea water, etc. The differences between them are mainly a matter of impurities, or the presence of different substances in the water. Rain water and other types of fresh water, usually have a very low concentration of salts and other substances, and therefore are very poor conductors. Sea water, on the other hand, has a much higher concentration of salts. The average salt concentration for sea water is about 35‰. Therefore it is a decent conductor. By comparison

Water type	Electric conductivity(µS/cm)
Rain water	5-30
Ground water	30- 2000
Sea water	45000-55000

Table 2.1: Salinity table [2]

silver and copper have a conductivity in the order of 10^7S/m.

Rain drops are a very variable parameter. Many different types of rain exists, but common for them all are that they need to have a certain weight in order to leave the clouds. This weight is determined directly by the size of the

drop. The distance a rain drop can fall before evaporating is also determined by its size. For a rain drop with a diameter of 20 µm evaporation will happen after about 3 cm. Hence drops need to be much bigger in order to reach the Earth's surface. A drop with a diameter of 200 µm will evaporate after about 150 m and is a good measure for the smallest diameter a rain drop can have. The most common rain drop diameters range from 1 mm to 4 mm. Table 2.2 shows the distribution of rain drop sizes and types.

Rain drop type	Average diameter d (mm)	Volume V(µL)
Small drops	0.1	$0.5 \cdot 10^{-3}$
Typical drops	1	0.5
	3	14.2
	4	33.5
Big raindrops	6	113.1

Table 2.2: Rain drop sizes [2]

Based on this data it was decided that drops with a volume of 10, 50 and 100 µl should be studied in this work.

2.2 Water droplets in electric fields

2.2.1 Geometry of water droplets

A water droplet is usually spherical when no electric field is present [3]. In this case the interfacial tension,γ, of the droplet will keep it spherical unless the gravitational forces becomes to big, i.e. when $\Delta\rho g << \gamma/R_0^2$. For a spherical water droplet with radius R_0 the pressure difference across the surfaces is give by the Young-Laplace equation:

$$\Delta p = \gamma \left(\frac{1}{R_1} + \frac{1}{R_2} \right) = 2\frac{\gamma}{R_0} \tag{2.1}$$

This means that smaller droplets are more likely to remain stable and spherical then larger droplets. When an electric field is applied to the droplet an extra term appears in the pressure calculation. This is the electrostatic pressure generated by the electric field on the droplet. This additional pressure

leads to deformation of the droplet. The droplet becomes stretched in the direction of the electric field. In other words the droplet becomes a spheroid. In order to understand how the electric field affects the droplet it is important to know the geometry of ellipses and spheroids. In addition to the definitions

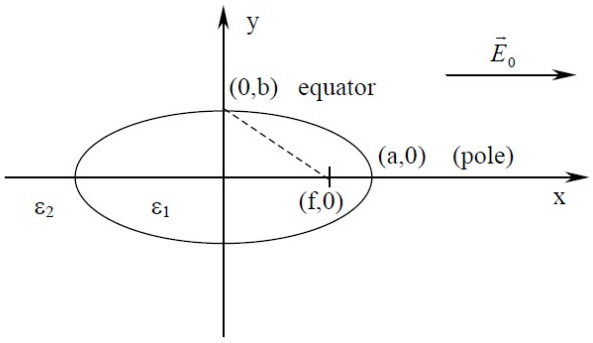

Figure 2.1: The basic geometry of an ellipse, where a and b are the semi axes and f marks the focal point

given inn figure 2.1 an ellipse is described by its eccentricity. Eccentricity is defined as the ratio of the distance between the two focal points of the ellipse and the length of the ellipse.

$$e = \frac{2f}{2a} = \frac{f}{a} \tag{2.2}$$

Eccentricity can also be given found by using the length of the semi axis:

$$e^2 = 1 - \frac{b^2}{a^2} \tag{2.3}$$

From this we can define a relationship between the semi axis:

$$\alpha = 1 - e^2 = \frac{b^2}{a^2} \tag{2.4}$$

An ellipse has two curvature radii, R_1 and R_2 that are defined as follows:

$$R_1 = a^2 b^2 \left(\frac{x^2}{a^4} + \frac{y^4}{b^4} \right)^{3/2}, \tag{2.5}$$

Position	R_1	R_2	$\left(\frac{1}{R_1}+\frac{1}{R_2}\right)$
(a,0)	$a^{-1}b^2$	$a^{-1}b^2$	$2ab^{-1}$
(0,b)	a^2b^{-1}	b	$ba^{-2}+b^{-1}$

Table 2.3: The values of the two curvature radii at (a,0) and (0,b)

$$R_2 = b^2\left(\frac{x^2}{a^2}+\frac{y^4}{b^4}\right)^{1/2}. \tag{2.6}$$

The main border condition in this system is that the droplets volume must remain constant. This means that the following applies:

$$\frac{4}{3}\pi R_0^3 = \frac{4}{3}\pi abc \tag{2.7}$$

Here R_0 is the radius of the spherical droplet and a, b and c are the semi axis of the spheroidal droplet. In a spheroid c will usually be equal to either a or b, depending on the type of spheroid in question, hence we get:

$$ab^2 = R_0^3 \tag{2.8}$$

by inserting (2.8) into (2.4) we get:

$$a = R_0\alpha^{-\frac{1}{3}} \tag{2.9}$$

and

$$b = R_0\alpha^{\frac{1}{6}} \tag{2.10}$$

2.2.2 Conducting water droplets in electric fields

In 1964 Taylor [4] developed a theory for describing conducting water droplets in electric fields. In his theory he states that the pressure difference across the surfaces are the same on all parts of the droplet surfaces. Therefore it is only necessary to study the pressure difference at two points. In order to simplify the calculations it is best to calculate the pressure at the poles and equator of the spheroid. Water droplets become elongated in the field so we are dealing with a prolate spheroid that has $c = b$. For water droplets

in an electric field eq (2.1) gets an extra contribution from the electrostatic pressure, $p = \frac{\epsilon_0}{2}E^2$. At the pole, (a,0), this becomes,

$$\Delta p_{pol} = \gamma\left(\frac{1}{R_1} + \frac{1}{R_2}\right) + \frac{\epsilon_0}{2}E_{pol}^2 = \gamma \cdot 2ab^{-2} + \frac{\epsilon_0}{2}E_{pol}^2 \tag{2.11}$$

and at the equator we get,

$$\Delta p_{eq} = \gamma\left(\frac{1}{R_1} + \frac{1}{R_2}\right) + \frac{\epsilon_0}{2}E_{eq}^2 = \gamma \cdot (ba^{-2} + b^{-1}) \tag{2.12}$$

At the equator the electric field normal to the surfaces is zero. At (a,0) the electric field is,

$$E = E_0\left(\frac{b^2}{a^2}\left(\frac{1}{2}e^{-3}ln\left(\frac{1+e}{1-e}\right) - e^{-2}\right)\right)^{-1} = \left(\frac{b^2}{a^2}I_2\right)^{-1} \tag{2.13}$$

where

$$I_2 = \frac{1}{2}e^{-3}ln\left(\frac{1+e}{1-e}\right) - e^{-2}. \tag{2.14}$$

Since $\Delta p_{pol} = \Delta p_{eq}$ we find that,

$$\begin{aligned} 2\gamma ab^{-2} + \frac{1}{2}\epsilon E^2 &= \gamma(ba^{-2} + b^{-1}) \\ \Rightarrow \frac{\epsilon}{\gamma}E_0^2 &= \sqrt{2}\frac{1}{a}\left(\frac{b}{a}\right)^2\left(2 - \frac{b}{a} - \left(\frac{b}{a}\right)^3\right)\cdot I_2 \end{aligned} \tag{2.15}$$

by inserting eq (2.9),with $\alpha = \left(\frac{b}{a}^2\right)$, into eq (2.15) we get an expression of the deformation of the droplet as a function of the electric background field E_0, i.e. the field when there is no droplet present.

$$E_0\sqrt{\frac{2r_0\epsilon}{\gamma}} = 2\cdot\left(\frac{b}{a}\right)^{\frac{4}{3}}\left(2 - \frac{b}{a} - \left(\frac{b}{a}\right)^3\right)^{\frac{1}{2}} I_2 \tag{2.16}$$

The expression under the square root on the left hand side is the electric Weber number. It represents the relationship between the electrostatic and

the capillary pressure. The right hand side is a pure geometric description of the droplets semi axis. When the droplet ratio a/b becomes greater then 1,9 the electrostatic pressure exceeds the capillary pressure and the droplet will break up. [3] The critical value of the electric field is then:

$$E_c = 0,648\sqrt{\frac{\gamma}{2\epsilon r_0}} \tag{2.17}$$

By plotting a/b as a function of $E_0\sqrt{\frac{2r_0\epsilon}{\gamma}}$, the theoretical expansion of a free water drop in an electric field, E_0, can be determined.

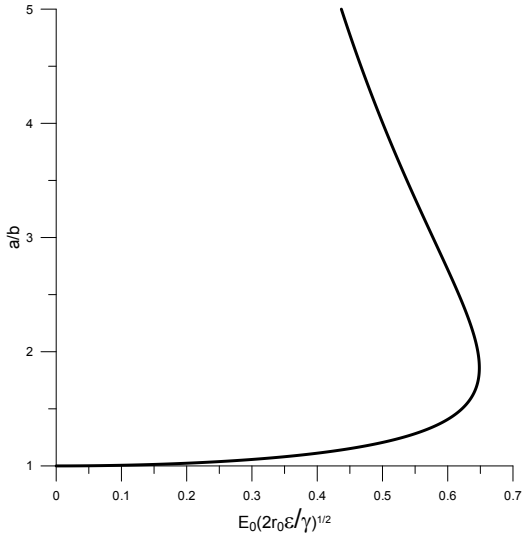

Figure 2.2: The critical value for expansion is visible here as the point where the plot changes direction

2.2.3 Dielectric water droplets in electric fields

Most water droplets have to low permittivity to be considered conducting, an extension of the theory applied to dielectric droplets is necessary. In a conducting water droplet, the electric field inside the droplet is zero. In a dielectric droplet on the other hand, there is an electric field inside the droplet that must be taken into consideration when making calculations. This internal field will contribute to the pressure situation across the interface. The

internal field can be found by solving Laplace's equation with prolate spherical coordinates [3]

$$E_i = E_0 \left[1 - \left(1 - \frac{\epsilon_d}{\epsilon}\right)(1 - e^2)I_2\right]^{-1} \tag{2.18}$$

here ϵ_d is the permittivity of the drop and ϵ is the permittivity of the bulk phase, e.g air. The same concept applies here as for the conductive droplet, the pressure difference across the pole is the same as across the equator.

$$E_0\sqrt{\frac{2r_0\epsilon_0\epsilon}{\gamma}} = 2\left(\frac{a}{b}\right)^{\frac{2}{3}}\left(2 - \frac{b}{a} - \left(\frac{b}{a}\right)^3\right)^{\frac{1}{2}}\left|\frac{1}{1 - \frac{\epsilon_d}{\epsilon}} - \frac{b^2}{a^2}I_2\right| \tag{2.19}$$

The permittivity of water is about, ϵ_d=80 and the sounding, air, has permittivity ϵ=1. Inserting this data into eq 2.19 and plotting the stretching a/b as a function of $E_0\sqrt{\frac{2r_0\epsilon}{\gamma}}$ gives the graph seen in figure 2.3.

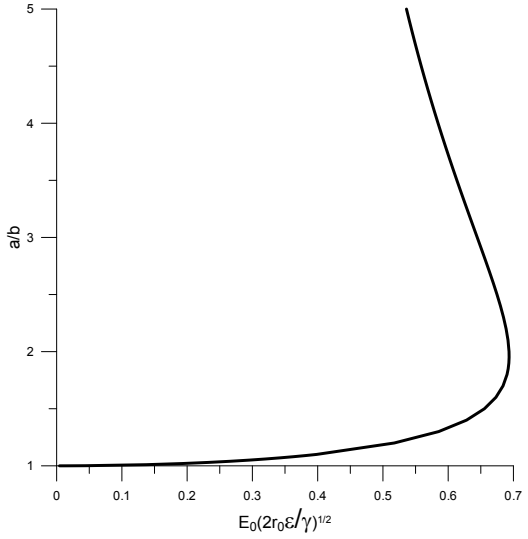

Figure 2.3: The critical value for expansion is visible here as the point where the plot changes direction

The difference between figure 2.2 and 2.3 is very small, due to the relative small difference in permittivity between water and air.

2.3 Sessile droplets in electric fields

2.3.1 Description of a sessile water drop

A water drop placed on a hydrophobic insulating surface will have a shape similar to that showed in figure 2.4

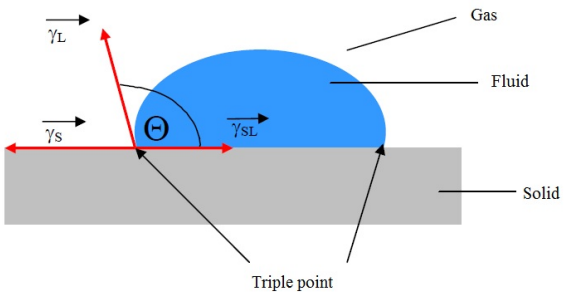

Figure 2.4: Water droplet on a solid surface [2].

The system consists of three mediums, gass(G), liquid(L) and solid(S). The contact angle, θ, is defined as the angle the surface of the droplet makes with the surface of the solid at the point where all three mediums meet. This point is called the triple point. The three mediums interact with each other over three interfaces liquid/solid(LS), gas/solid(GS) and gas/liquid(GL). The line of triple points around the droplet is called the contact line. [5]. When a water droplet is placed on a solid surface the force equilibrium is provided by the Young's equations [6]. The parameters used for this situation are the surface tension between gas and solid γ_{GS}, the surface tension between liquid and solid γ_{LS}, the surface tension between gas and liquid γ_{GL} and the contact angle θ.

The equilibrium situation is described by the following equation:

$$\gamma_{GS} - \gamma_{LS} = \gamma_{GL} \cdot cos\theta \tag{2.20}$$

Usually the surface tension between the liquid and the air, γ_{GL}, is known and θ is measurable by studying a picture or video of the droplet. That leaves two unknowns in the system, but it is the difference between the two,$\gamma_{GS} - \gamma_{LS}$

that is interesting here. There are two main forces that controls this situation, adhesion and cohesion. These forces always exist when there is an interaction between a liquid and a solid [2].

Adhesion work is given by the following equation:

$$W_{ad} = \gamma_{GS} + \gamma_{GL} - \gamma_{LS} \tag{2.21}$$

Cohesion work is given by:

$$W_c = 2\gamma_{GL} \tag{2.22}$$

When a liquid and a solid comes into contact, the surface tension and the interfacial tension compete with each other in order to become as small as possible. This leads to a spreading of the liquid. Spreading is defined as the difference between the adhesion work and the cohesion work.

$$S = W_{ad} - W_c = \gamma_{GS} + \gamma_{GL} - \gamma_{LS} - 2\gamma_{GL} = \gamma_{GS} - (\gamma_{GL} + \gamma_{LS}) \tag{2.23}$$

When $S > 0$ there will be spreading and for $S \leq 0$ we will not have spreading. So spreading occurs when we have a greater adhesion between the solid and liquid then the cohesion of the liquid. When we have complete wetting of the surface the spreading is so large that the droplet becomes a liquid film on the surface of the solid.

A. Moukengué Imano and A.Beroual present a description of the deformation of a water droplet on a solid surface under the effects of an electric field [5]. In this paper they present an excellent derivation of the forces involved and how they affect the droplet. This derivation will be reproduced here.

2.3.2 Description of the system

The presence of an electric field can lead to changes in the droplet shape. The changes in shape can be characterized by the motion of:

- the gas liquid interface I_{GL} in the direction normal to the interface.
- the contact line L_{GLS} parallel to the solid surface and normal to the contact line.

The deformation of the droplet happens generally in the same direction as the electric field. The deformation is caused by changes in the interface energies U and the negative work W on the gas/liquid interface and contact line. The variation of Gibbs free energy, G, of both the interface I_{GL} and the contact line L_{GLS} is given by:

$$dG = dU - dW, \tag{2.24}$$

with

$$dU = \gamma_{GS} dA_{GS} + \gamma_{LS} dA_{LS} + \gamma_{GL} dA_{GL}, \tag{2.25}$$

$$dW = \sum f_I dV_I, \tag{2.26}$$

here γ is the interfacial tension and A is the area of a given interface. The sum $\sum f_I$ is the sum of all external forces per unit area, this corresponds to the external actions on the system. Consider a small motion of I_{GL} and L_{GLS} that may not obey any kinetic law. The line element of L_{GLS} sweeps a surface element dA_L during the virtual motion of the contact line L_{GLS}. Similarly I_{GL} has its virtual motion characterized by the volume variation dV_I. With this in mind eq (2.25) becomes:

$$dU = (\gamma_{GS} - \gamma_{LS} - \gamma_{GL} cos(\theta_C))\, dA_L + \gamma_{GL}(\vec{\nabla} \cdot \vec{n}) dV_I \tag{2.27}$$

$\vec{\nabla} \cdot \vec{n}$ is the mean curvature of I_{GL}, θ_C is the contact angle and $\vec{n}$ is a unit vector normal to I_{GL}. Inserting eqs (2.26) and (2.27) into eq 2.24 yields

$$dG = (\gamma_{GS} - \gamma_{LS} - \gamma_{GL} cos(\theta_C))\, dA_L + \left(\gamma_{GL}(\vec{\nabla} \cdot \vec{n}) - \sum f_I\right) dV_I \tag{2.28}$$

When the change in Gibbs free energy of I_{GL} and L_{GLS} is zero, the equilibrium state of the system is given by the following conditions:

$$\left(\gamma_{GL}(\vec{\nabla} \cdot \vec{n}) - \sum f_I\right) = 0, \tag{2.29}$$

$$\gamma_{GS} - \gamma_{LS} - \gamma_{GL} cos(\theta_C) = 0. \tag{2.30}$$

2.3.3 Governing equations for the gas/liquid interface

The following external forces per unit area interact with the gas/liquid interface in the equilibrium state:

- The force F_γ due to interfacial tension
- The force F_p due to pressure differences
- The force F_E due to the electric stress
- The force F_g due to the gravity

The effects of the viscosity of the water are neglected here. Since all the interaction of the external forces occur normal to I_{GL}, eq (2.29) can be written as:

$$\vec{n} \cdot \left(\sum f_I - \gamma_{GL}(\vec{\nabla} \cdot \vec{n}) \right) = 0. \tag{2.31}$$

This means that

$$\vec{n} \cdot \sum f_I = \vec{F_P} + \vec{F_E} + \vec{F_G}, \tag{2.32}$$

and

$$\vec{F_\gamma} = -\vec{n} \cdot \gamma_{GL}(\vec{\nabla} \cdot \vec{n}). \tag{2.33}$$

The mean curvature of a gas/liquid interface can, according to Laplace-Young equation for a sessile drop, be written as:

$$\vec{\nabla} \cdot \vec{n} = \frac{1}{R_1} + \frac{1}{R_2} \tag{2.34}$$

where R_1 and R_2 are the principal radii of curvature at any point of I_{GL}. For an axisymmetric interface I_{GL}. According to Bashforth-Adams's approximation,R_1 and R_2 can be expressed through the equations:

$$\frac{1}{R_1} = \frac{d\theta}{ds} \tag{2.35}$$

$$\frac{1}{R_2} = \frac{sin(\theta)}{r} \tag{2.36}$$

where s is the arc length of droplet profile in an r-z plane of an axisymmetric droplet shape. The variation of s can be written as:

$$ds = \sqrt{dr^2 + dz^2} \tag{2.37}$$

Inserting eqs (2.35) and (2.36) into (2.34), the mean curvature of I_{GL} can be expressed with the help of a series of ordinary differential equations as a function of the arc length s:

$$\vec{\nabla} \cdot \vec{n} = \frac{d\theta}{ds} + \frac{sin(\theta)}{r}, \tag{2.38}$$

$$\frac{dr}{ds} = cos(\theta), \tag{2.39}$$

$$\frac{dz}{ds} = sin(\theta). \tag{2.40}$$

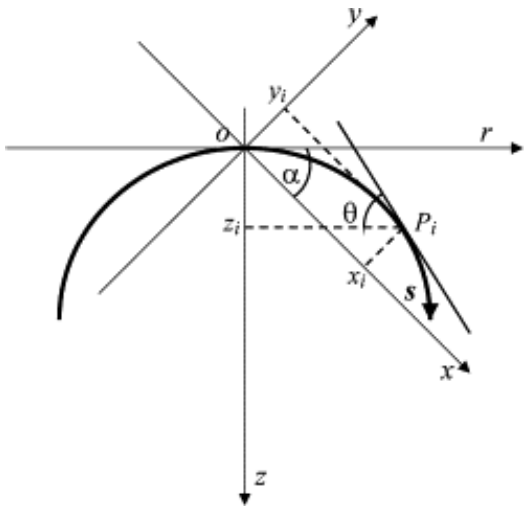

Figure 2.5: r-z plane of an axisymmetric droplet shape [5]

2.3.3.1 The force due to the interfacial tension

The interfacial tension applies a force per unit area on the gas/liquid interface. Inserting eq (2.38) into eq (2.33) gives the following expression for this force:

$$\vec{F_\gamma} = -\vec{n} \cdot \gamma_{GL} \left(\frac{d\theta}{ds} + \frac{sin(\theta)}{r} \right). \tag{2.41}$$

In a three-dimensional coordinate system (x, y, z), as seen in figure 2.5, the system of differential equations (2.38)-(2.40) becomes:

$$\vec{F_\gamma} = -\vec{n} \cdot \gamma_{GL} \left(\frac{d\theta}{ds} + \frac{sin(\theta)}{\sqrt{x^2 + y^2}} \right), \tag{2.42}$$

$$\frac{dx}{ds} = cos(\theta)cos(\alpha), \tag{2.43}$$

$$\frac{dy}{ds} = cos(\theta)sin(\alpha), \tag{2.44}$$

and

$$\frac{dz}{ds} = sin(\theta). \tag{2.45}$$

θ and α are the coordinates in the spherical coordinate system given in figure 2.5. They are bound by the following values: $0 \leq \theta \leq \pi$ and $-\pi/2 \leq \alpha \leq \pi/2$

2.3.3.2 The forces due to the gravity and pressure difference

The effect of gravity on the shape of the droplet occurs parallel to z-axis and normal to the surface element of I_{GL}.

$$\vec{F_g} = \vec{n} \cdot g\Delta\rho z, \tag{2.46}$$

where g is the acceleration due to gravity, $\Delta\rho$ is the density difference across I_{GL} and z is the vertical coordinate of the application point.

The force per unit area due to the pressure difference Δp over the interface I_{GL} is:

$$\vec{F_p} = \vec{n} \cdot \Delta p \tag{2.47}$$

2.3.3.3 Force due to electric stress

The electric stress will create a force $\vec{F_E}$ that will contribute to the deformation of the sessile droplet. The difference of the electrostatic pressure across is the cause of this force. For a surface element of the gas/liquid interface with a very small thickness, the Maxwell tensor is reduced to the following electrostatic pressure.

$$\vec{F_E} = \vec{T_G} + \vec{T_L} + \vec{T_{GL}} \tag{2.48}$$

$\vec{T_G}$ and $\vec{T_L}$ are the electrostatic pressure on both parallel interface sides and $\vec{T_{GL}}$ is the difference of the electrostatic pressure normal to the thickness of the considered area element. By neglecting the thickness of the interface eq (2.48) becomes:

$$\vec{F_E} = \vec{T_G} + \vec{T_L} = T_n\vec{n} + T_t\vec{t} \tag{2.49}$$

$\vec{n}$ and $\vec{t}$ are the normal and tangential unit vectors to the element respectively. T_n and T_t are the normal and tangential component of $\vec{F_E}$ respectively. By regarding the droplet as conducting, the Maxwell tensors can be written as:

$$\vec{T_G} = \epsilon_G(\vec{n_G} \cdot \vec{E_G})\vec{E_G} - \epsilon_G\frac{\vec{n_G}}{2}\vec{E_G}^{\,2}, \tag{2.50}$$

$$\vec{T_L} = \epsilon_L(\vec{n_L} \cdot \vec{E_L})\vec{E_L} - \epsilon_L\frac{\vec{n_L}}{2}\vec{E_L}^{\,2}, \tag{2.51}$$

with

$$\vec{E_G} = E_{Gn} \cdot \vec{n_G} + E_{Gt} \cdot \vec{t_G}, \tag{2.52}$$

$$\vec{E_L} = -E_{Ln} \cdot \vec{n_L} + E_{Lt} \cdot \vec{t_L}, \tag{2.53}$$

$$\vec{n_G} = -\vec{n_L} = \vec{n}, \tag{2.54}$$

$$\vec{t_L} = \vec{t_G} = \vec{t}, \tag{2.55}$$

where E_n and E_t are the normal and tangential components of the corresponding electric field strength respectively, see figure (2.6). The electric permittivity of the medium is given by ϵ.

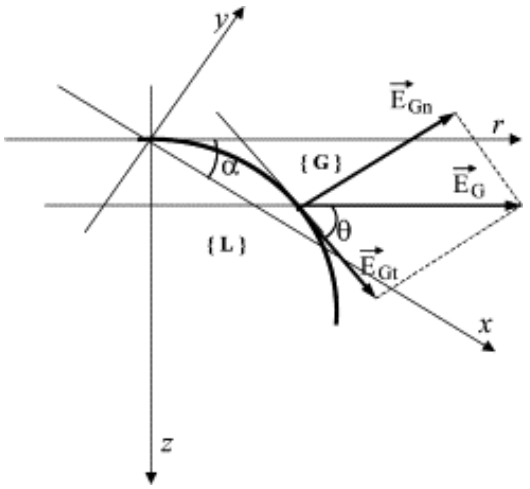

Figure 2.6: Normal and tangential components of the electric field strength at the gas/liquid interface in the surrounding gas [5]

Inserting eqs (2.54) and (2.55) into eqs (2.50)-(2.53) gives:

$$\vec{T_G} = \epsilon_G(\vec{n} \cdot \vec{E_G})\vec{E_G} - \epsilon_G \frac{\vec{n}}{2}\vec{E_G}^{\,2}, \tag{2.56}$$

$$\vec{T_L} = \epsilon_L(\vec{n} \cdot \vec{E_L})\vec{E_L} - \epsilon_L \frac{\vec{n}}{2}\vec{E_L}^{\,2}, \tag{2.57}$$

$$\vec{E_G} = E_{Gn} \cdot \vec{n} + E_{Gt} \cdot \vec{t} \tag{2.58}$$

and

$$\vec{E_L} = -E_{Ln} \cdot \vec{n} + E_{Lt} \cdot \vec{t}. \tag{2.59}$$

By substituting (2.58) and (2.59) into (2.56) and (2.57) and adding them together an expression for $\vec{F_E}$ is obtained. Using eq (2.49) expressions for the normal and tangential component of $\vec{F_E}$ can by found.

$$T_n = \frac{\epsilon_G}{2}(E_{Gn}^2 - E_{Gt}^2) - \frac{\epsilon_L}{2}(E_{Ln}^2 - E_{Lt}^2), \tag{2.60}$$

$$T_t = \epsilon_G E_{Gn} E_{Gt} - \epsilon_L E_{Ln} E_{Lt}. \tag{2.61}$$

The following boundary conditions related to the electric field strength and displacement for a charged droplet apply in this situation:

$$\left\| \vec{n} \times \vec{E} \right\| = E_{Gt} - E_{Lt} \Rightarrow E_{Gt} = E_{Lt} \tag{2.62}$$

$$\left\| \vec{n} \cdot \epsilon \vec{E} \right\| = \epsilon_G E_{Gn} - \epsilon_L E_{Ln} = \sigma \tag{2.63}$$

By inserting these conditions into eqs (2.60) and (2.61) they become

$$T_n = \frac{1}{2}\left(\left(\epsilon_G E_{Gn}^2 - \frac{1}{\epsilon_L}(\epsilon_G E_{Gn} - \sigma)^2\right)(\epsilon_G - \epsilon_L) E_{Gt}^2\right) \tag{2.64}$$

and

$$T_t = \sigma E_{Gt} \tag{2.65}$$

where σ is the surface charge density on the droplet. The surface charge density is influenced by the electric conductivity, κ, in the following manner:

$$\frac{d\sigma}{dt} + \frac{\kappa_L}{\epsilon_L}\sigma = \left(\frac{\kappa_L}{\epsilon_L} - \frac{\kappa_G}{\epsilon_G}\right)\epsilon_G E_{Gn} \tag{2.66}$$

If the transient state characterized by the accumulation or the evacuation of surface charge is neglected compared to the established mode the solution to eq (2.66) is

$$\sigma(t) = \left(1 - \frac{\epsilon_L \kappa_G}{\epsilon_G \kappa_L}\right)\epsilon_G E_{Gn} \tag{2.67}$$

then eqs (2.64) and (2.65) become

$$T_n = \frac{1}{2}\left(\left(1 - \frac{\epsilon_L \kappa_G^2}{\epsilon_G \epsilon_L^2}\right)\epsilon_G E_{Gn}^2 - (\epsilon_G - \epsilon_L)E_{Gt}^2\right) \tag{2.68}$$

and

$$T_t = \left(1 - \frac{\epsilon_L \kappa_G}{\epsilon_G \kappa_L}\right)\epsilon_G E_{Gn} E_{Gt} \tag{2.69}$$

In a three dimensional coordinate system (x, y, z) with an undistorted electric field parallel to the solid surface the tangential and normal components of $\vec{E_G}$ can be written as:

$$E_{Gn} = E_G sin(\theta) cos(\alpha) \tag{2.70}$$

$$E_{Gt} = E_G cos(\theta) cos(\alpha) \tag{2.71}$$

Substituting eqs (2.70) and (2.71) into eqs (2.68) and (2.69) and rearranging gives:

$$T_n = (cos(\alpha)^2(k_1 + (k_2 - k_1))(cos(\theta))^2), \tag{2.72}$$

and

$$T_t = k_3(cos(\alpha))^2 cos(\theta) sin(\theta) \tag{2.73}$$

with

$$k_1 = \frac{\epsilon_L E G^2}{2}\left(1 - \frac{\epsilon_L \kappa_A^2}{\epsilon_A \kappa_L^2}\right), \tag{2.74}$$

$$k_2 = \frac{\epsilon_G E_G^2}{2}\left(\frac{\epsilon_L}{\epsilon_G} - 1\right), \tag{2.75}$$

and

$$k_3 = \epsilon_g E_G^2 \left(1 - \frac{\epsilon_L \kappa_G}{\epsilon_G \kappa_L}\right). \tag{2.76}$$

2.3.4 Dimensionless formulation of the equation of the shape of the gas/liquid interface

The principal equation of the sessile droplet system is given by the following expression:

$$-\vec{n} \cdot \gamma_{GL}(\vec{\nabla} \cdot \vec{n}) + \vec{n} \cdot \delta p + \vec{n} \cdot T_n + \vec{n} \cdot g\delta\rho z = 0. \tag{2.77}$$

By substituting eqs (2.41), (2.46), (2.47) and (2.72) into eq (2.77) and rearranging the following equation is obtained:

$$\frac{d\theta}{ds} = -\frac{sin(\theta)}{\sqrt{x^2+y^2}} + \frac{\delta p}{\gamma_{GL}} + \frac{(cos(\alpha)^2}{\gamma_{GL}}(k_1 + (k_2 - k_1)(cos(\theta))^2) + \frac{g\delta\rho z}{\gamma_{GL}} \tag{2.78}$$

In order to generalize the equation the system of differential equations made up of eqs (2.43)-(2.45) and (2.78) can be written in the following non-dimensional form:

$$\frac{d\theta}{dS} = 2 - \frac{sin(\theta)}{\sqrt{X^2+Y^2}} + B_O Z + W_{eO} E_n^2 (cos(\alpha))^2 (K_1 + K_2 (cos(\theta))^2). \tag{2.79}$$

$$\frac{dX}{dS} = cos(\theta)cos(\alpha), \tag{2.80}$$

$$\frac{dY}{dS} = cos(\theta)sin(\alpha) \tag{2.81}$$

and

$$\frac{dZ}{dS} = sin(\theta) \tag{2.82}$$

with $S = bs$, $X = bx$, $Y = by$ and $Z = bz$, where

- $b = \frac{1}{R_Apex}$ is the curvature at the origin of coordinates;
- $B_O = \frac{g\delta P}{b^2\gamma_{GL}} = \frac{g\delta\rho R_{Apex}^2}{\gamma_{GL}}$ is the non-dimensional Bond number;

- $W_{eO} = \frac{\epsilon_G E_{G\infty}^2}{2b\gamma_{GL}} = \frac{\epsilon_G E_{G\infty}^2 R_{Apex}}{2\gamma_{GL}} = \frac{\epsilon_G U_G^2}{2bd^2\gamma_{GL}} = \frac{\epsilon_G U_G^2 R_{Apex}}{2d^2\gamma_{GL}}$ is the non-dimensional electric Weber number for homogeneous electric field;
- E_n is a non-dimensional form factor for a homogeneous electric field;
- U_G is the potential difference between both electrodes;
- d is the gap between the electrodes;
- R_{Apex} is the radius at the origin of coordinates(Apex);
- $K_1 = 1 - \frac{\epsilon_L \kappa_G^2}{\epsilon_G \kappa_L^2}$ and $K_2 = \frac{\epsilon_L(\kappa_G^2 + \kappa_L^2)}{\epsilon_G \kappa_L^2} - 2$ are non dimensional electric constants.

2.3.5 Calculation of the form factor for electric field

A deformed sessile droplet on a dielectric solid surface disturbs the homogeneous electric field provided by both electrodes under certain conditions. This disturbance of the background is attributed to the field enhancement at the tips of the droplet and it is a positive feedback phenomena that causes further distortion of the droplet.

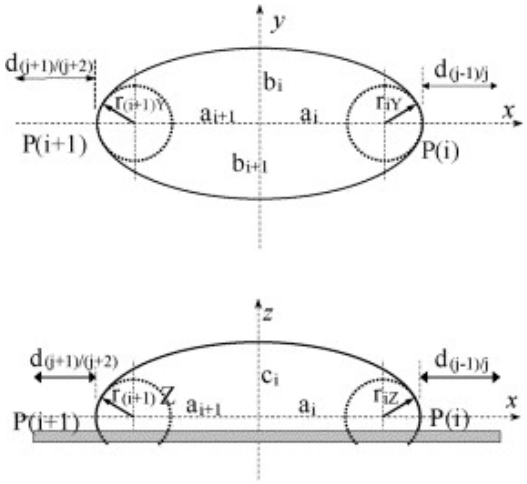

Figure 2.7: Front and top views of a single droplet between two electrodes [5]

The normal component of the field strength E_1 at one of the elementary points on the droplet tip P_1 can be expressed as

$$E_1 = \frac{U_1}{\eta_1 d_1} \tag{2.83}$$

with

$$U_1 = U \frac{d_1}{d - a_1 - a_2} \tag{2.84}$$

η_1, U_1 and d_1 are respectively a corresponding inhomogeneity factor for the droplet tip P_1, a virtual potential difference and the shortest distance between the droplet tip P_1 and the opposite electrode. Using the assumption of a plane condenser made up of a conducting screen with thicknesses a_1 and a_2 on eq (2.83), we get the following expression for E_1:

$$E_1 = \frac{U}{d} \frac{1}{\eta_1 (1 - \frac{a_1 + a_2}{d})} \tag{2.85}$$

The screen is inserted between both electrodes. U is the potential difference and d is the distance between the electrodes. a_1 and a_2 represents the semi-axes of the droplets in the direction of pole P_1 and P_2 respectively, see figure 2.7. The general form factor in this case is

$$E_{n1} = \frac{1}{\eta_1 (1 - \frac{a_1 + a_2}{d})} \tag{2.86}$$

this form factor has a double influence from the dimensions of the droplet, through the semi-axes and through eta_1. For multiple droplets this becomes

$$E_{ni} = \frac{1}{\eta_i \left(1 - \frac{\sum_{i=1}^{m} a_i}{d}\right)} \tag{2.87}$$

where η is an inhomogeneity factor for each tip of the droplet calculate according to a (p,q) geometry. Let R and r be the radii of the major and minor spheres of a sphere-sphere configuration, respectively. Then the following geometry applies in (p, q) space:

$$p = \frac{d + r}{r} \tag{2.88}$$

$$q = \frac{R}{r} \tag{2.89}$$

with $R = \infty$ for a sphere-plane configuration. In order to calculate η, we assimilate the radius of curvature at the tip of the droplet to a virtual sphere. A small water droplet can be assumed to have the form of the cap of an ellipsoid of revolution. Elongation of a droplet will decrease the distance between two droplets and thereby enhance the field. Therefore E_n will have to be determined by an iterative computation in order to get the correct results.

In a sphere-plane configuration the inhomogeneity factor can be approximated to,

$$\eta = c_1 e^{c_2/(p+c_3)} \tag{2.90}$$

when there is sphere-sphere configuration, equal radii for the spheres on both sides of the droplet, the inhomogeneity becomes:

$$\eta = \frac{4}{p + \sqrt{p^2 + 8}} \tag{2.91}$$

with $c_1 = 30.51 \cdot 10^{-2}$, $c_2 = 17.78$ and $c_3 = 40.96 \cdot 10^{-1}$.

2.3.6 Electrohydrodynamic phenomena

Electrohydrodynamics describes the changing movements(dynamic) of a water droplet (hydro) under the influence of an electric field(electro) [7]. The movement of a droplet starts at a critical electric stress level. This level depends on surface and liquid properties. S, Keim et al described the different motions a sessile droplet will experience in an electric field in their article "Experimental investigations on electrohydrodynamic phenomena at single droplets on insulating surfaces". These descriptions were very useful in this thesis work.

When a droplet is exposed to an alternating electric field the droplet will experience transient surface structures. These structures change within milliseconds and repeat with each half period of a sinusoidal voltage, see figure 2.8a. This change in surface structure can be seen as a trembling, or oscillation, of the surface. This trembling depends on the voltage level, liquid parameters, distances to neighboring droplets and the material properties of the surface.

The electric field enhancement is strongest at the triple points. [7] Because of this the triple points will move in the direction of the field, towards the electrodes. When the width of the droplet increases, the height must naturally be decreased. This leads to a flatter droplet with a sharper contact angle, see figure 2.8b.

When to droplets are placed close together the triple points may move towards each other when an electric field is applied. Because of this a very thin water path may be created between the two droplets. If the distance between the droplets is very small, a collapsing of the two drops into one larger drop might be observed, see figures 2.8c and 2.8d.

A large drop can in some cases be separated into two distinct drops. In some cases a small satellite droplet will be left behind in the middle of the two newly separated droplets. Small satellite droplets can also be ejected from a larger droplet when no separation takes place. This is shown in figures 2.8e and 2.8f

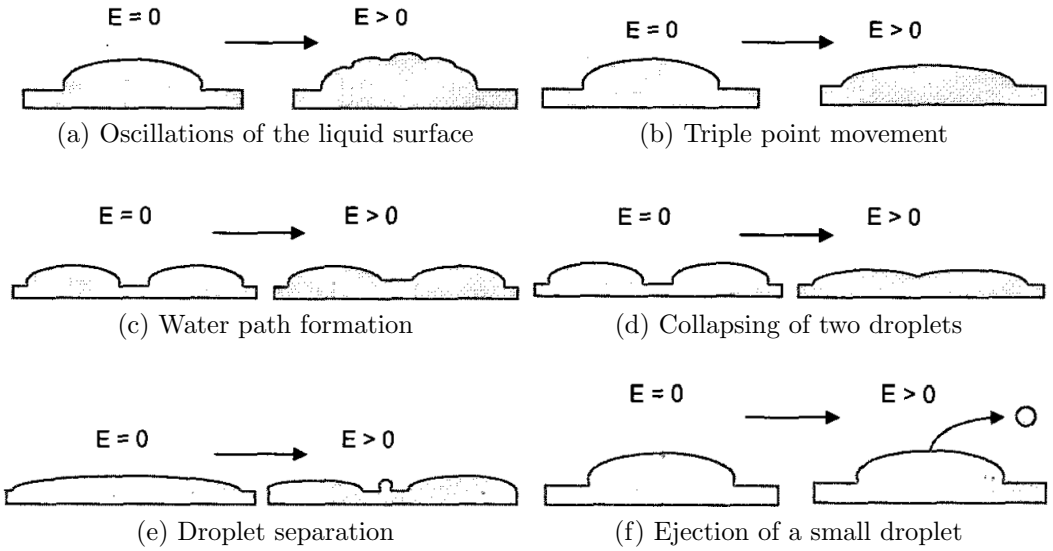

(a) Oscillations of the liquid surface (b) Triple point movement

(c) Water path formation (d) Collapsing of two droplets

(e) Droplet separation (f) Ejection of a small droplet

Figure 2.8: Overview of basic movement patterns for electrically stressed droplets [7]

2.4 Partial discharges

2.4.1 Definition

Partial discharges (PD) are localized electrical discharges within an insulation system, restricted to only a part of the dielectric material, and thus only partially bridging the electrodes. [8] They are one of the main sources of faults and aging in an insulation system. [9]. There are many different types of discharges that are included in the term partial discharges. Internal discharges occurs in voids or cavities within the solid insulation. Surface discharges appear at the boundary of different materials in the insulation. Corona discharges are related to discharges in gaseous dielectrics and are caused by strong inhomogeneous electric fields. All of these discharges can lead to damage on the material through the energy impact of high energy electrons or accelerated ions. When the electrons and ions interact with the insulation material there will be chemical changes.

Droplets on surfaces increase the chances of surface discharges [10]. Surface discharges are therefore given the most attention in this work. When experiments were conducted great effort was taken to remove the other types of discharges from the system. The internal discharges were reduced by making the samples as void free as possible. Corona was avoided by careful positioning of the components used in the experiment and good grounding.

2.4.2 Surface and corona discharges

Surface discharges occur in the boundary of two different dielectric mediums when there is a sufficiently strong electric field tangential to the boundary.

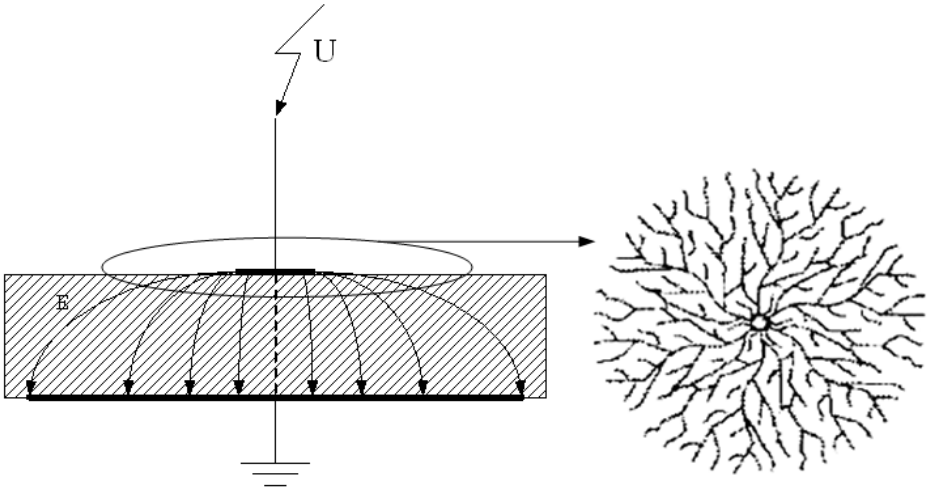

Figure 2.9: Left: Due to high electric stress along the surface, there could be surface discharges near the electrode. [11] Right: A typical pattern created by a surface discharge on an insulating material. (Lichtenberg figure) [11]

At sufficiently high electric stress there will be discharges in the area around the high voltage electrode, see figure 2.9.The discharges will evolve from corona discharges to treeing. Surface discharges occur most often at the ends of insulations [11].

Corona discharges are discharges at sharp edges. Around these edges the electric field becomes very large and the air can become ionized. The discharges

normally occur when the voltage reaches its positive or negative peek.

2.4.3 Detection of partial discharges

The detection of PDs is based on the energy exchanges that occur in the discharge. [8]. The energy exchanges manifest themselves in a number of ways:

1. Electrical impulse currents
2. Dielectric loss
3. E.M. radiation in the form of light
4. Sound, a hissing and sparking noise can be heard when discharges occur
5. Increased gas pressure
6. Chemical reactions

In this thesis work PDs were detected by studying the electrical impulses. This method is the most successful and most frequently used method of detecting discharges.

2.4.4 Tracking

Tracking is the most important degradation factor for electric insulation. It occurs when the surface of the insulation is covered by a contaminant and moisture, i.e. sea water. This mixture of water and contaminants will work as an electrolyte and conduct current. When the fluid is conducting current, there will be a heat development that will lead to evaporation. This will again lead to the creation of dry zones. At the edge of such dry zones the electric field will be very strong and we will have partial discharges. These discharges can lead to destruction of the insulation, by turning parts of it to carbon. If this process is allowed to continue without treatment it can lead to the creation of conductive tracks from one electrode to another. Such a track would lead to an electrical arcing along the surface of the insulation [12].

2.4.5 Erosion

Erosion is closely linked to tracking, but it demands more energy. In this case, some of the material disappears due to the energy developed in the partial discharges. Here, as in the tracking case, the disappearance of isolating material is due to it being converted to carbon. When this happens repeatedly in the same location we get eroded areas in the shape of cracks [12].

2.4.6 Partial Discharges from water drops on insulating surfaces

When a water droplet is placed in an electric field, the field in the area around the drop will be intensified. The largest enchantment will be at the triple point. [10]. Due to this field intensification the drop will be elongated in the direction of the field and there will be more field intensifications. These intensifications lead to partial discharges that can lead to damages to the insulation. [13]. The starting point of the partial discharges, the inception voltage, is dependent on a number of factors. Water droplet conductivity, polymer surface roughness, whether the surface is hydrophobic or hydrophilic, droplet volume and the positioning of the droplet with respect to the electrodes all contribute to the inception voltage level [14].

Chapter 3

Experimental work

3.1 Droplet shape and size on glass fiber enforced epoxy composite

The shape and size of the water droplets were the most important factors in this study. Water will naturally evaporate from a surface at room temperature, the glass fiber enforced epoxy composite has also shown a large capacity for water absorption [1]. In other words the water droplet will naturally change its shape over time. For the studies to be accurate it was important to know how long the droplet would keep its original shape. The change in droplet volume was studied by placing one 100 µL droplet on the surface of the sample, and leaving it there for one hour. A picture was taken with a digital microscope every two minutes. The width and height of the droplets in the pictures were then measured and used to calculate a simple approximation of the volume. The change in droplet volume as a function of time, was then calculated and used to determine the time constraint for the electric studies. In order to determine whether the evaporation into air or absorption into the sample was the larger factor, a droplet was placed on a PET surface. The same type of test was conducted on this droplet. Similar studies were conducted for 10 and 50 µL droplets.

3.2 Partial discharge measurement

3.2.1 Test sample

The test sample used in the partial discharge experiments, was based on the design used by S. Keim [2]. The dimensions of the sample were modified in order to create a similar electric field at the surface of the sample, as that observed in the actual turbine. Figure 3.1 shows a 3D drawing of the sample with the final measurements.

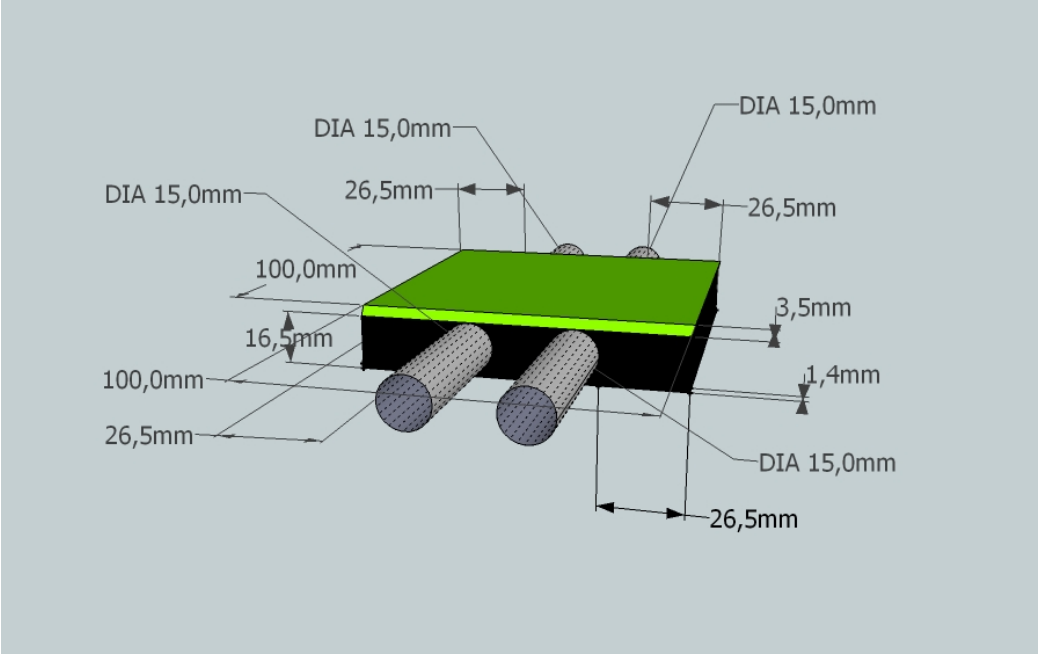

Figure 3.1: 3D drawing of the test sample with the correct measurements. The left electrode was connected to high voltage and the right to ground.

The sample consisted of two electrode tubes cast in place with a filler epoxy and a 3.5 mm thick glass fiber enforced epoxy composite surface piece. In the experiments one of the electrodes was grounded and the other connected to the high voltage source. The sample was created by casting the epoxy in a mold that had been designed in advance. The mold was designed by Hans Helmer Sæternes from SINTEF and constructed in NTNUs natural science

workshop. The construction of the mold was delayed several weeks. In order to avoid losing to much time a simple mold of plastic and wood was created. This mold had the same dimensions with regards to electrode diameter and distance between the two electrodes. The molding process was the same with both the steel and plastic mold. The epoxy was first dried under stirring in a vacuum chamber and then pored into the mold were the electrodes had already been placed. The glass fiber enforced epoxy composite surface piece was placed on top of the electrodes. The sample was then placed in a heat locker for 18 hours. During these 18 hours the filler epoxy expanded. The plastic mold could not keep the filler epoxy in place during this expansion. Because of this sample created with this mold did not have a flat surface and the sides of the sample became uneven. The stainless steel mold was designed to prevent this from happening. It had bolts and screws that were used to keep pressure on the epoxy during the solidification. The stainless steel mold worked very well and this sample was used for all the PD experiments in this thesis. The sample created with the plastic mold was used to determine droplet evaporation and what voltage levels PDs were likely to occur. It was also used for the tracking and erosion test.

3.2.2 Measurement setup

The classic setup for measuring partial discharges are given in figure 3.2

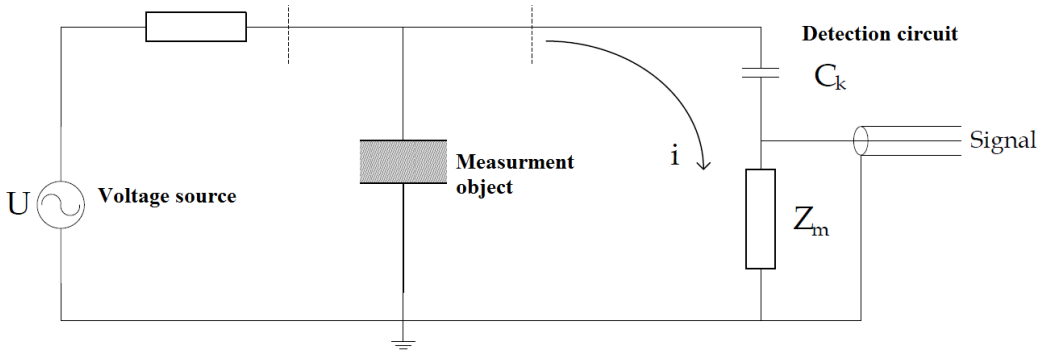

Figure 3.2: Setup for PD measurement

The coupling capacitor (C_k) is placed in series with the measurement impedance (Z_m). These two are again connected in parallel with the measurement ob-

ject and the high voltage source. The coupling capacitor is included in order to provide a low impedance circuit for the high frequency signals, the measurement impedance is insert to ensure that the currents from the discharges will provide a measurable voltage [9]. In order to register the discharges it is necessary to use a high frequency measuring apparatus. The transient voltage pulses that are detected over the measuring impedance are very small and have a high frequency. The coupling capacitor should have a capacitance equal or greater than the capacitance of the measuring object. This is required in order to get a good sensitivity to the measurements.

The noise limits used during the measurement of the partial discharges in this work was set to 1.5 pC. The electronic measurements where preformed with a MPD 600 system from Omicron Mtronix technologies. The equipment consists of a measuring shunt that is plugged in to the detection part of the circuit. The measuring shunt is connected to a measuring unit that records and registers the size of the high frequency voltage signals created by the partial discharges. The measurement unit converts these analog results to digital data that is sent with fiber optics to a computer for processing, see figure 3.3.

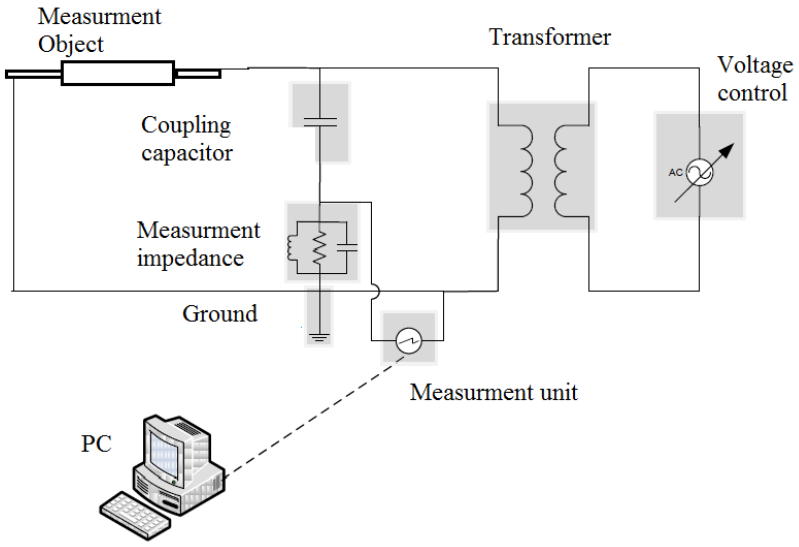

Figure 3.3: Sketch of the measurement setup used for detection and measurement of partial discharges.

All the high voltage equipment and the test sample where placed in a metal cage that was grounded according to the safety protocols given by SINTEF. In addition to the PD measuring equipment a digital microscope was placed inside the cage. The microscope filmed the behavior of the droplets during testing.

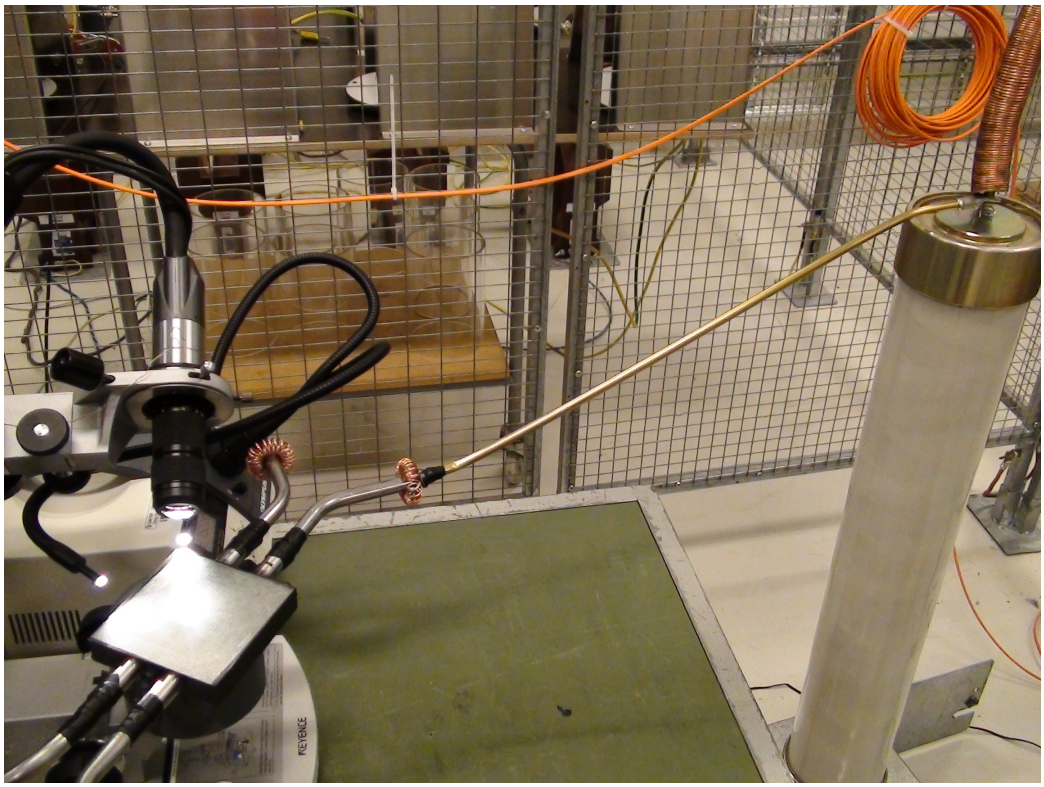

Figure 3.4: This is a picture of the experimental setup used to conduct the PD measurements

Figure 3.2 shows how close the microscope lens was to the sample during testing. The two black wires seen in the figure are LED lights that were used to improve the focus of the microscope recordings. In order to decrease the chance of discharges in the system, all metal components were grounded and the microscope was placed on the grounded side of the sample. The voltage electrode was connected to the capacitor and high voltage source with a slightly flexible brass rod. That gave the setup some freedom of movement. This was useful when positioning the microscope for optimal focus.

3.2.3 Calibration

Before an accurate measurement of the size of the partial discharges could be recorded the measurement circuit had to be calibrated. The calibration was done by applying a known charge over the test object. The applied charge leads to a current being created in the measurement circuit. This current provided a voltage fluctuation over the measurement impedance. The relation between the known charge and the voltage fluctuation provided the calibration factor.

When voltage was applied to the measurement circuit, the partial discharges were registered as small transient voltage impulses over the measurement impedance. From the calibration factor the apparent charge can be calculated.

$$Q_{Apparent} = \frac{Q_k}{U_k} \cdot U_{PD} = k \cdot U_{PD} \tag{3.1}$$

where $Q_{Apparent}$ is the apparent charge, Q_k is the charge applied during the calibration, U_k is the voltage fluctuation due to the calibration charge and U_{PD} is the voltage fluctuation due to the partial discharge.

3.2.4 Measurement preparations

Before each measurement the microscope was positioned and the focus was adjusted in order to obtain the best possible recordings of the droplet behavior. If the microscope lens was placed to close to the high voltage electrode it would cause interference in the partial discharge measuring. Since the surface absorbed water each consecutive test was conducted on a separate location.

The preparation of each test started by choosing a new location, or one that had not been used in a while, and focusing the microscope on this location. Then the voltage was set to the relevant levels in order to determine whether or not there were any discharges in the system when there was no droplet present. If there were any discharges, adjustments were made to the setup. These adjustments usually involved moving the microscope lens.

When a discharge free setup had been found a small metal sphere of known dimensions, was placed on the surface. A picture was taken of the sphere and the diameter measured. This was done in order to have a known reference of the size and shape of the water drops for this particular situation. Since the microscope was in a different location each time it was impossible to have one reference length for all the experiments. When all the preparations were done, a water droplet with a volume of 10, 50 or 100 µl was placed with a syringe at the desired location. A stopwatch was used to mark the time when the droplet was placed on the surface, when the microscope recording was started, when the PD recording was started and any other major changes to the setup.

3.2.5 Measurement procedure

Measuring of the partial discharge behavior of the droplet was done in incremented steps. The voltage was first set to 6 kV and left there for about one minute. The voltage was then raised to 8 kV and left there for one minute. This was repeated until the voltage reached 16 kV. The total measuring time was about six minutes. Based on the data obtained in the evaporation test it was determined that within this time frame all three droplet sizes retained there original form to an acceptable degree. The time of each increase in the voltage level was noted with the stopwatch. The Mtronix measurement system provided data of the time and size of every discharge recorded in the setup. The voltage level was also noted and the relation between a discharge and the phase of the AC voltage. After each test the PD data was exported to a MATLAB file and the video recording of the droplet behavior was studied closely.

From the video recording the dimensions of the droplets and the distances between them were obtained. By comparing the PD data and the video of the droplet all the aspects of the droplet behavior were covered. The video recording was always started a few seconds before the PD recording, due to placement issues. The stopwatch was used to mark when the voltage was raised in the video recording and the time difference between the two recordings.

The initial voltage level was chosen to be 6 kV, since this was around the same value as the voltage would be in the turbine. The final value of 16 kV was chosen after initial tests confirmed this as a voltage level with guarantied partial discharges for deionized droplets with a volume of 50 and 100 µl. Water droplets with a volume of 10 µl did not produce any discharges and were therefore left out of future measurements.

3.2.6 Droplet positioning

M.G. Danikas et al conclude that droplet conductivity, surface roughness, droplet volume and the relative position of the droplets, all affect the behavior in an electric field [14]. The droplets they used had a volume of 200 µl. In order to determine the effects of the positioning of the droplets multiple droplets were placed in several different patterns on the test surfaces. For the most part the droplets were placed in a single line, normal to the electrodes, but two of the setups used, had drops in three different rows. A similar approach was used in this thesis.

Initially one drop was placed in the center of the sample, see figure 3.5a. In order to investigate the effects of multiple droplets, several droplets of the same size were placed in a line between the two electrodes. M.G. Danikas et al used laser light in order to get the highest degree of accuracy in the placement of the droplets. In the absence of such lasers PET sheets, with round holes in them, were used to position the droplets in these experiments. Four basic patterns were made, see fig3.5. The holes in the PET sheets were much larger than the droplets. This was necessary in order to avoid breaking the droplets during placement, the average width of a 100 µl droplet when placed on the surface was 8 mm. This meant that all the droplets in the situations in fig 3.5 were fairly far from each other, and there was little chance of two droplets collapsing. Therefore four additional situations were studied. One where two drops were placed as close to each other as possible in the middle of the electrodes, one where a third droplet was placed between the two droplets in fig 3.5c, one where two droplets were placed between the two droplets in fig 3.5b and one where five 50 µl droplets were placed from electrode to electrode. For the five droplet situation the volume was reduced

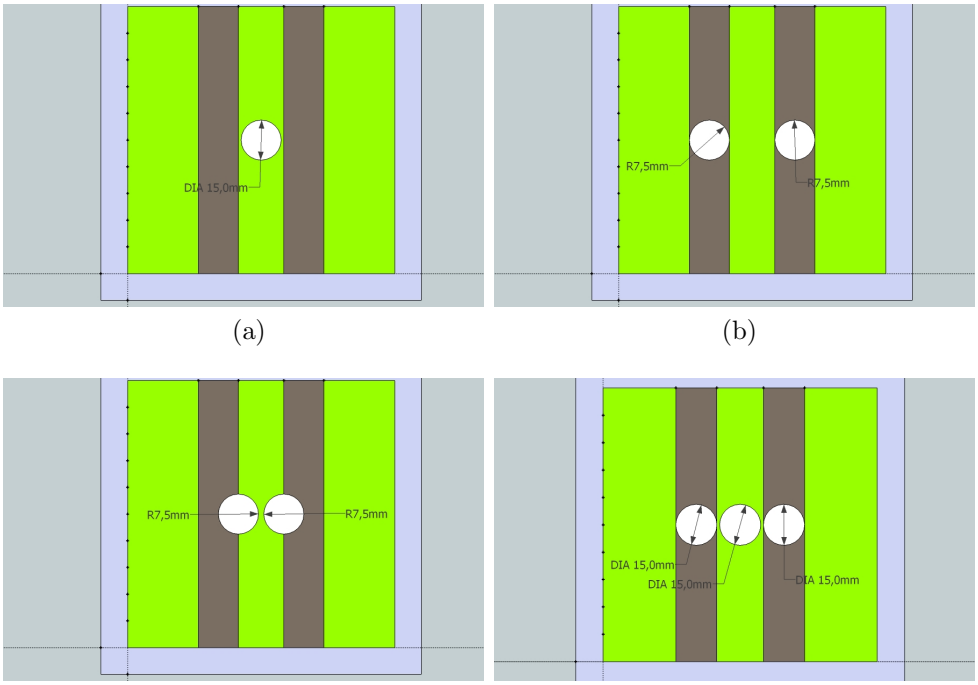

(a) (b)

(c) (d)

Figure 3.5: Models of the PET sheets used to place the water droplets on the surface.

to 50 µl in order to keep the droplets between the electrodes.

For each of these seven multi droplet situations two increment test was conducted. Since the droplet placement was done by hand there were small differences in the distances between the droplets and the shape of individual droplets. Therefore all the tests were conducted twice. The final test with deionized water was a random placement of small drops over a large surface area. This was supposed to simulate an actual situation of rain drops on the surface.

In earlier work it was discovered that the presence of water changed the dielectric constant of the samples [1]. This meant that conducting an increment

Situation	Symbol
No droplet	D0
1 droplet placed in the middle of the two electrodes	D1
2 droplets one over each electrode	D2_1
2 droplets one over the edge of each electrode	D2_2
2 droplets in the middle of the electrodes	D2_3
3 droplets one over each electrode and one in the middle	D3_1
3 droplets one over the edge of each electrode and one in the middle	D3_2
4 droplets	D4
5 droplets	D5

Table 3.1: This table lists the different setups used in the droplet experiments and the symbol used to describe them later in the thesis.

test at the same spot on the sample repeatedly, might lead to different results when water was absorbed into the sample. In order to determine whether or not, this had an effect on the PDs an additional test was conducted. In this test a drop was left on the surface for 30 min after an increment test was conducted. A new drop was then placed on the exact same location and the test was conducted again. The process was then repeated a final time.

3.2.7 Artificial salt water test

When testing the droplet behavior for salt water droplets, only 100 µl droplets where used. First one drop was placed in the middle of the electrodes and tested in the same manner as the deionized water droplets. Afterwards the surface was cleaned with water and the test repeated. In addition three droplets were placed close together in a line, the D3_2 setup, and tested for partial discharges.

When the salt water droplets dried up, the salt is left behind. Five tests were conducted in order to determine if this had an effect on the PD behavior. First three droplets were left on the surface to dry. When the droplets had dried, three new droplets were placed in the same place as the originals. The leftover salt created a mold for the droplets to form in. Therefore the second set of droplets, had nearly the same shape as the first once had the end of

the first measurement. The drying test on the three droplets were conducted twice, and all the PD behavior of all three setups were recorded.

In order to simulate sea spray on the surface, and to provide data for the following tracking test, a large number of small artificial sea water drops was spread out over the surfaces and left to dry. Three measurements were conducted. One on a clean surface, and two after the drops had been left to dry.

3.2.8 Oil saturated samples

The main goal of this thesis work was to determine if the presence of oil would have an effect on the discharges in the system. The oil used was the same oil that was used in the SmartMotor turbine. In previous work the diffusion procedure of the oil into the sample had been studied. The effect of the oil on the electric permittivity of the sample had also been measured [1]. The droplets in all the tests were placed on the glass fiber enforced epoxy composite surface. In order to fill the surface piece with oil, the sample was left face down in an oil bath and placed in a heat locker for two weeks. The plan was to have the heat locker hold a temperature of 30 °C, but this was not possible in the heat locker that was available at the time of testing. The temperature inside would not drop lower then 40 °C. The problem here, was that at a higher temperature the saturation level is higher [1]. When the sample was taken out into a room with a significantly lower temperature, than in the heat locker, the diffusion onto the surface would be much greater than desired. In order to negate this error, the sample was placed in a freezer for 10 min immediately after it was taken out of the heat locker. When the sample had cooled, it was wiped clean and put back into the PD measuring setup.

Similarly to the salt water tests, PDs were measured for both one and three drops. First deionized water was investigated before the PD measuring was concluded with salt water droplets on an oil saturated sample. After all the measurements, the sample was put back into the oil bath so that it could be saturated once more.

3.2.9 Liquid-Contaminant Inclined-Plane Tracking and Erosion test

Based on the ASTM international Standard Test Methods for Liquid-Contaminant Inclined-Plane Tracking and Erosion of Insulating Materials [15], a test was conducted to determine whether any long term damages occurred due to discharges. The test was conducted on an 45° inclined test sample. Two tests were conducted, one dry sample and one saturated with oil. The same test sample used in the previous oil tests was used for the oil saturated part, and the sample made with the plastic mold was used for the dry test. In the test salt water was dripped on to the top of the sample and allowed to flow down to the bottom. The sample made with the plastic mold was longer than the one made with the steel mold. The extra length made it possible to conduct four parallels at once. The dripping speed was one droplet every 10 s and the droplets where about 50 µl.

The voltage level used in the experiment was determined based on the data obtained from the multiple droplet experiments conducted with both deionized water and artificial salt water. In the salt water test it was observed that small discharges occurred at about 6 kV, when there was dry salt present. This was very interesting, since this is the same voltage level as in the actual turbine.

To simulate the actual situation on the surface of the turbine, it was decided that the wetting of the surface should be periodic. First droplets were dripped onto the surface for 16 h. Afterwards the dripping was turned off and the salt water was left to dry for 8 h with the voltage on. For the first seven days the voltage was set to 6.2 kV. The artificial saltwater was dropped onto the inclined surface using a standard hospital drip bag. The bag was suspended above the test surface, which was placed above a clean bowl that collected the salt water after it had flown down the surface. By doing this any problems created by having saltwater on the floor of a high voltage area was avoided. Each of the hose ends were fasted in a set position before the start of the experiment. The sample was placed in spirit level so that each drop flowed separately and straight down, see figure 3.6, for the dimensions of the experiment.

Before the start of the experiment the roughness of the surface was measured. Three parallel lines where measured, one along each electrode and one in the middle of the electrodes. The water flowed normal to these lines and therefore it was easy to see both where erosion had happened and where the damage was largest. After the seven days the roughness was measured again. The experiment was then reset with a new voltage level. The new voltage was chosen to be at a level where PDs had definitely been observed for salt water, 10 kV. With the voltage at 10 kV, there was no doubt that discharges occurred. They could be both heard and seen, when the voltage was turned on. The change in surface roughness was measured twice more, at seven days intervals.

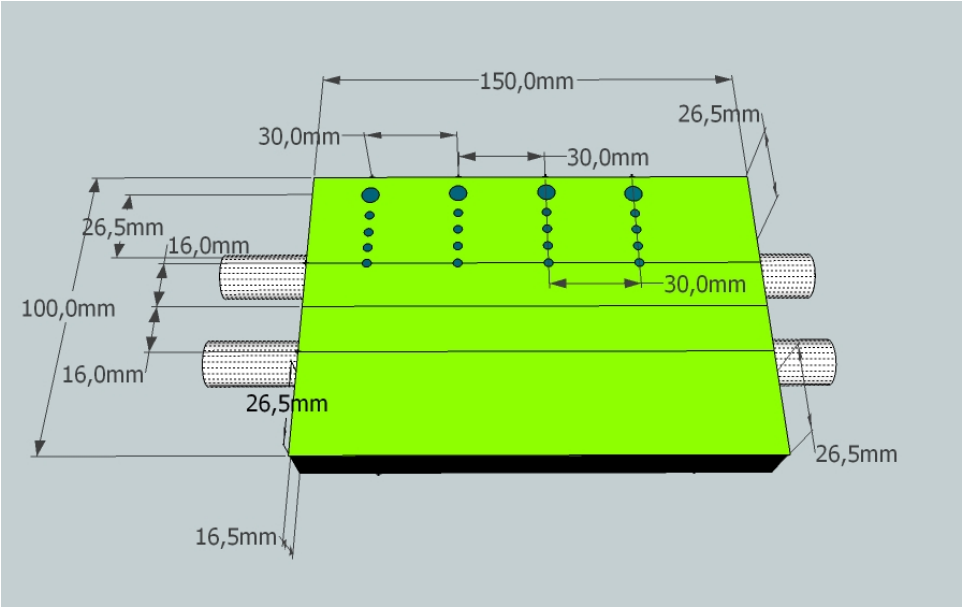

Figure 3.6: This figure shows the setup for the erosion test with proper dimensions. The horizontal lines represents lines where surface roughness was tested.

The oil saturated sample was treated similarly. Due to limited time, the oil saturated sample was only tested at 10 kV. By conducting the experiment at a higher voltage the odds of damages increased. The first surface roughness

measurement was done immediately after the oil saturated sample had been removed from the oil bath. The sample was then connected to the same setup used for the dry sample measurements, see figure 3.7.

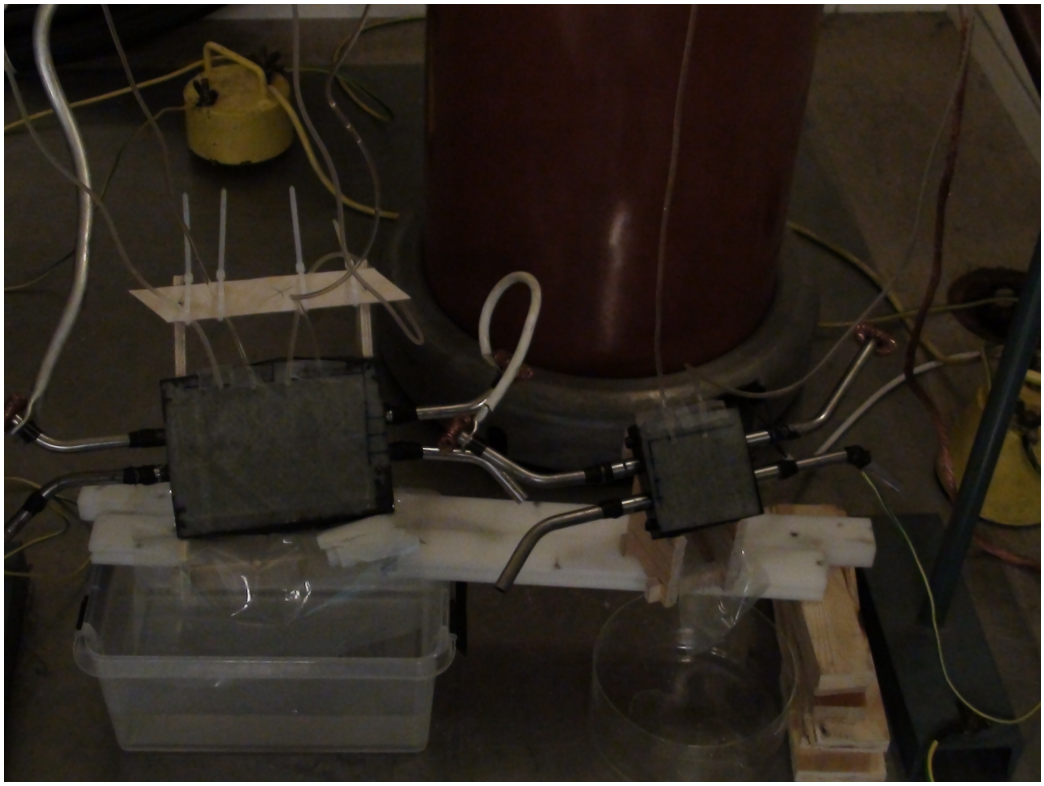

Figure 3.7: The oil saturated sample is the small one on the right. The upper electrodes are connected to high voltage and the lower to the ground. The bags containing the salt water are fastened to a beam above, and the ends of the hoses are taped in place at the top of the sample.

3.2.9.1 Surface roughness testing

The roughness of the surface of the samples was determined with a Mitutoyo Surftest SV-2100. The measuring was conducted by moving a small stylus over the surface of the sample and measuring the differences in surface height. A graph describing the shape of the surface was the end product of the measurements. All the data points from the graph could easily be exported to

another program for analysis.

When measuring the surface roughness for the erosion test, it was important to be able to conduct the measuring at the same location each time. This was difficult since the measurement apparatus had to be positioned manually. In order to minimize this error the starting position for the stylus was marked and each test was conducted twice. As seen in figure 3.6 the dripping lines where spread out over the entire width of the sample. In record the change in surface roughness around all four points, a measurement sample of 12.5 cm was required. By using this length there was sufficient information about the roughness on both sides of each dripping line. The Mitutoyo device had a maximum measurement length of 10 cm. In order to obtain an optimal measurement the apparatus required a start and finish segment of about1 cm, that would not be included in the final result. The reason for this start and finish segment was to ensure that the measured data was filtered correctly [16]. Hence the total length that would have been necessary to measure was 14.5 cm. In order to fix this the sampling was done in two segments. One with a total length of 9.5 cm and a sample length of 7.5 cm and one with a total length of 7 cm and a sample length of 5 cm.

Measurement of the surface roughness was conducted by first measuring the 9.5 cm segment. When a measuring sequence was finished the Mitutoyo device immediately returned the stylus to the starting position. After the first part had been measured twice, the whole setup was moved 7.5 cm. The second segment was then measured twice. By moving the setup 7.5 cm, the second segment was able to begin at about the same place as the first segment ended, thereby ensuring that there was no hole in the measurement.

Since the oil saturated sample was much smaller than the dry sample there were no problems with measuring the surface roughness. Due to the shorter surface there was only space for two dripping parallels for the oil investigations.

3.3 Simulations

In addition to the experiments a series of finite element method (FEM) simulations where conducted. Every situation studied in the experiments was simulated in COMSOL multiphysics. By using the dimensions obtained from the microscope recordings, the simulations became as realistic as possible. The most important factors in these simulations were the size of the droplets, the distances between them and the contact angle. The contact angle was determined by taking a close up picture of the droplet edge with the microscope. Getting the shape of the contact angle correct was the largest challenge in the simulation. These simulations are primarily a study of the droplets just before an expansion occurred. With the available equipment it was very difficult to create accurate models of the shape of a droplet after an expansion.

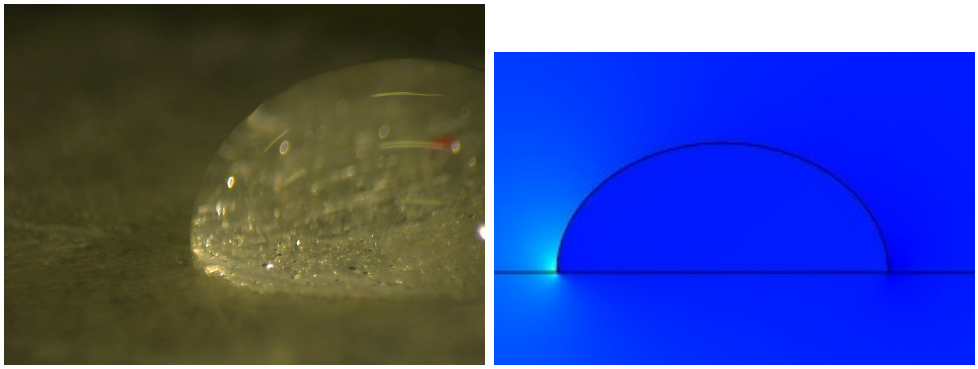

(a) Edge of 100 µl drop (b) COMSOL version of drop

Figure 3.8: This figure shows a closeup of the edge of a 100 µl droplet and the COMSOL figure that was made to match it.

As seen in figure 3.8a the droplet had a triple point angle of about 90°. This was matched in COMSOL by drawing an elongated ellipse and cutting it in half, as seen inn figure 3.8b. The simulations where conducted in 2D for simplicity. This was sufficient due to the symmetry of the setup. The simulations provided the electric field strength in the area around the electrodes and droplets. The most interesting area for study was at the droplet triple point, i.e. the interface between air, solid and water. The size of the electric field, in the direction parallel to the surface, was measured over the area where the droplets were placed. This data was transferred to MATLAB for

analysis and comparison with the experimental results.

In order to check the quality of these simulations the value of the field at the tip of one drop on the surface was compared to that expected from the method devised by Moukengué Imano et al [5]. Due to the slight difference between the two setups a direct comparison was not possible. Moukengué Imano et al had a more homogeneous field around their droplet, since they had placed the droplet in the middle of the electrodes. When the electrodes were embedded in the surface the shape of the field changed slightly. In order to solve this difference, the background field obtained in the COMSOL simulation was used instead of the simple model, of voltage difference divided by electrode distance, used by Moukengué Imano et al.

Chapter 4

Results

4.1 Deionized water samples

4.1.1 Experiments

The experiments conducted with the deionized water droplets gave a clear correlation between PD detection, droplet surface trembling and droplet expansion. In all the situations where PDs were detected, a trembling was observed on the surface of the droplets. The trembling and the PDs were always detected at about the same time. The voltage was adjusted in incremented steps and it was therefore easy to determine what voltage level the discharges started at. The data from the PD measuring device consisted of the size of the discharge in pC, the time and phase of each PD event and the voltage level over time during the measurement. In most cases the first PD events where recorded when the voltage was increased or a short time after a voltage increase. The voltage level that the first PD event was recorded at is called the inception voltage. Table 4.1 shows the inception voltages for all the deionized water droplets.

Situation	Inception voltage level (kV)
D0	No discharges
D1 100 µL	14
D1 100 µL moist surface	12
D1 50 µL	16
D1 10 µL	No discharges
D2_1 1st	No discharges
D2_1 2nd.	No discharges
D2_2 1st	16
D2_2 2nd	16
D2_3 1st	12
D2_3 2nd	12
D3_1 wide	16
D3_2 1st	12
D3_2 2nd	12
D4 1st	10
D4 2nd	10
D5 1st	8
D5 2nd	12
Multiple Droplets 1st	14
Multiple Droplets 2nd	6

Table 4.1: The inception voltage in all the situations tested.

When discharges were detected there was also an expansion of the droplet diameter. The direction of the expansions was the same as the direction of the E-field. Depending on the situation the expansion occurred before or after the first PDs were recorded. Some of the tests also had multiple expansions. In most cases the expansion happened before the discharges, since the expansion caused an even greater field enhancement at the edge of the droplet.

The size of the expansions were determined by measuring the change in droplet width from one edge to another. The widths of the droplets were measured by taking still pictures from the video recordings of the droplets. The pictures were taken immediately after the voltage had been increased, and at the start and finish of the experiment. Due to the limitations of the

microscope used in this work, the resolution of the pictures taken from the recordings was not the best. Therefore the measurement was not completely accurate, but the larger changes in width caused by the expansions, were easy to observe.

During the work on this thesis, several droplet setups were investigated. There were many similar trends in the different setups, and therefore a closer study of droplet behavior was limited to just two situations. The reason for this limited sample size was that the droplet behavior was the main focus point of this study, not quantification of parameters. The two chosen situations were one drop alone in the middle of the two electrodes, D1, and three drops in the narrow setup, D3_2. Each setup was investigated at least twice, the parallel chosen for close up study was the one that had the best microscope recording. One of the biggest challenges in the experimental work was to position the microscope. If the microscope was positioned to close to the sample, it would disturb the results of the discharge measurement. In some cases the droplets would expand outside of the microscope's field of vision. Figure 4.1 shows the change in droplet width as a function of voltage for one and three droplets of deionized water. Occasionally the droplets would expand further between the time when the voltage was raised to 16 kV and the end of the measuring sequence. This is shown in figure 4.1 as an extra point at the 16 kV mark.

The PD measuring software supplied by Mtronix noted the size, phase and time of every PD during an experiment. The voltage was recorded in fixed intervals regardless of whether or not there was a PD event. That meant that the number of data points recorded for the size of the PDs and the size of the voltage was different. Therefore it was difficult to compare the two sets of data directly. The correlation between voltage increase and change in PD behavior was essential to this study. In order to obtain this relation, it was necessary to manually locate the points where the voltage was increased. The voltage was increased manually by turning a large knob. Adjusting the voltage to the desired level usually took a few seconds. The time used to designate the voltage change was the start of the adjustment process, regardless of how long it took to obtain the desired level. Figure 4.2 shows the correlation between the size of the PDs and the voltage level for D1 and D3_2.

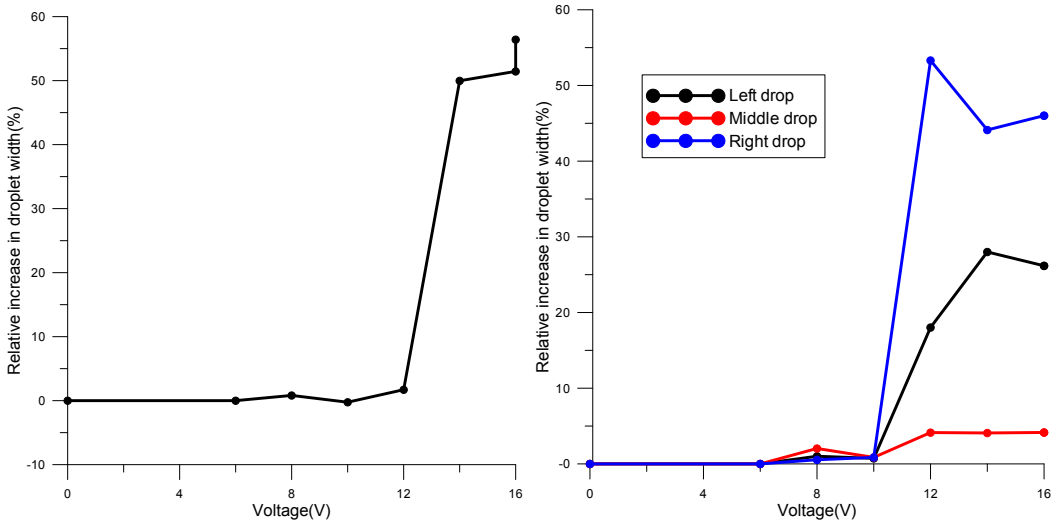

(a) D1 (b) D3_2

Figure 4.1: Change in droplet width, in % of the start width, as a function of voltage, for one and three droplets on a dry surface.

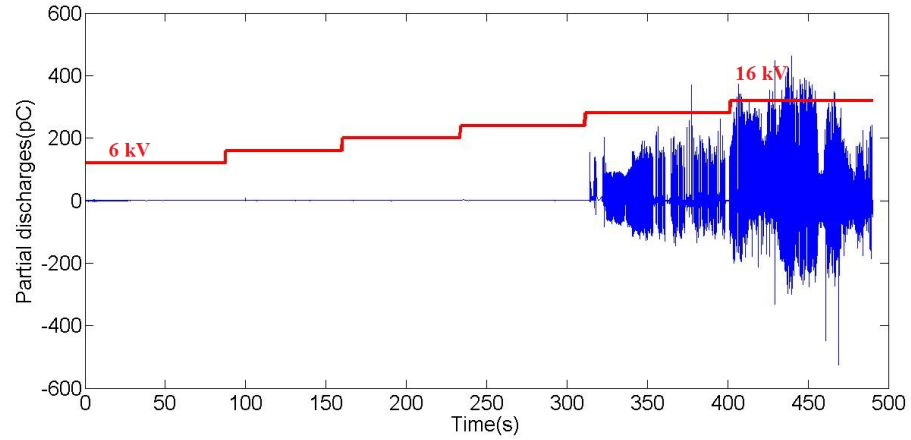

(a) D1

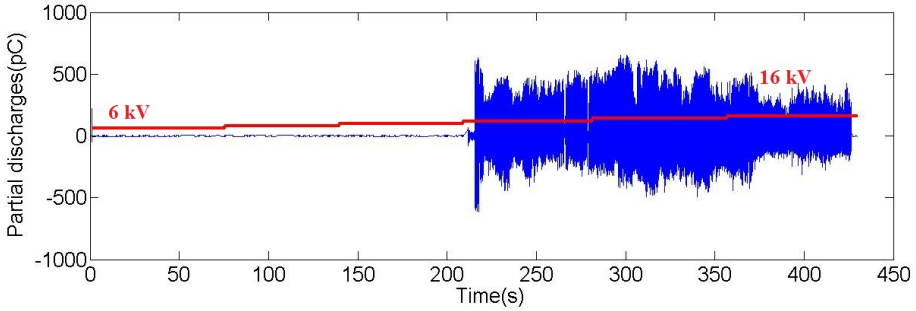

(b) D3_2

Figure 4.2: Time dependence of the PDs for the entire test. The red line represents the voltage levels used in the experiments. The voltage starts at 6 kV and increases by 2 kV in every step until it reaches 16 kV

Below are figures showing the PD behavior around the time an expansion occurred for one 100 µL and the second D3_2 situation. The sample of the PD data was 8 s long and shows the PD situation before and after the expansion. In addition to the size of the PD, figures 4.3 and 4.4 show when in the phase of the voltage the PDs occurred. The expansions occurred at 14 kV and 10 kV respectively. In the figures w represents the width of the droplets at the time the image was taken.

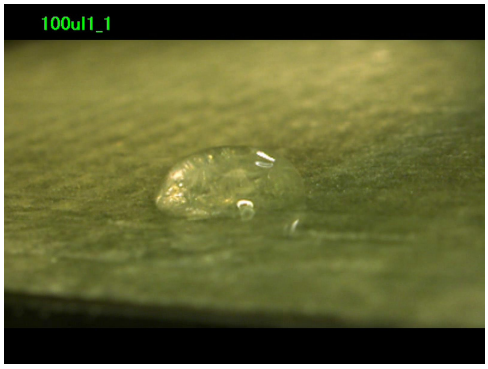

(a) Droplets at the start of the experiment. w=8.37 mm

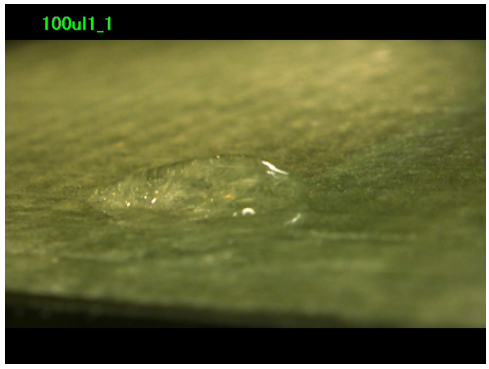

(b) Droplets right after the expansion w=12.34 mm

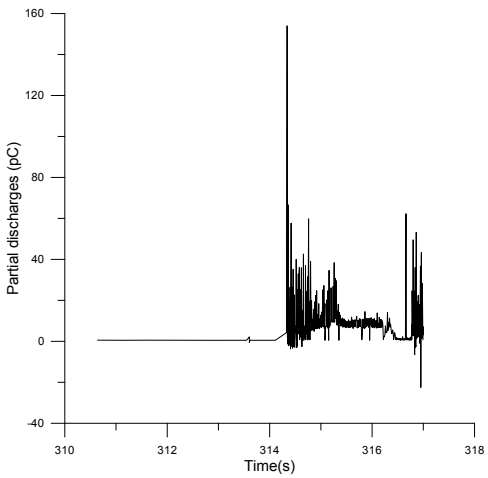

(c) Partial discharges as a function of time around the time of the expansion.

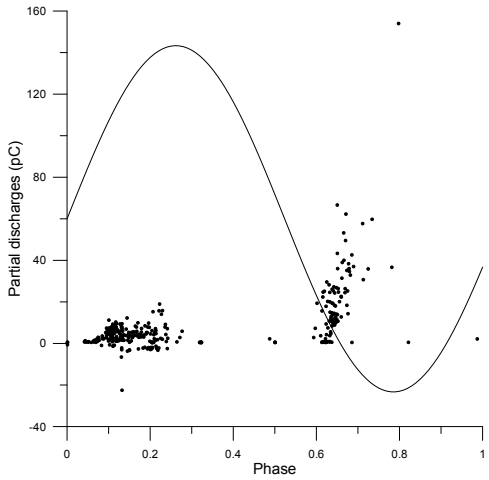

(d) The relation between each PD and the phase of the AC voltage.

Figure 4.3: The expansion of the droplet in the first D1 100 µL experiment.

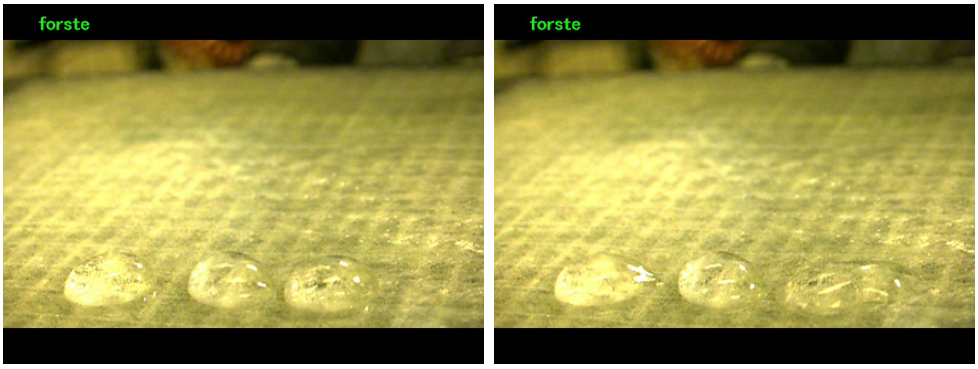

(a) Droplets at the start of the experiment. w_l=7.64 mm, w_m=7.29 mm and w_r=7.94 mm

(b) Droplets right after the expansion w_l=8.96 mm, w_m=7.52 mm and w_r=12.1 mm

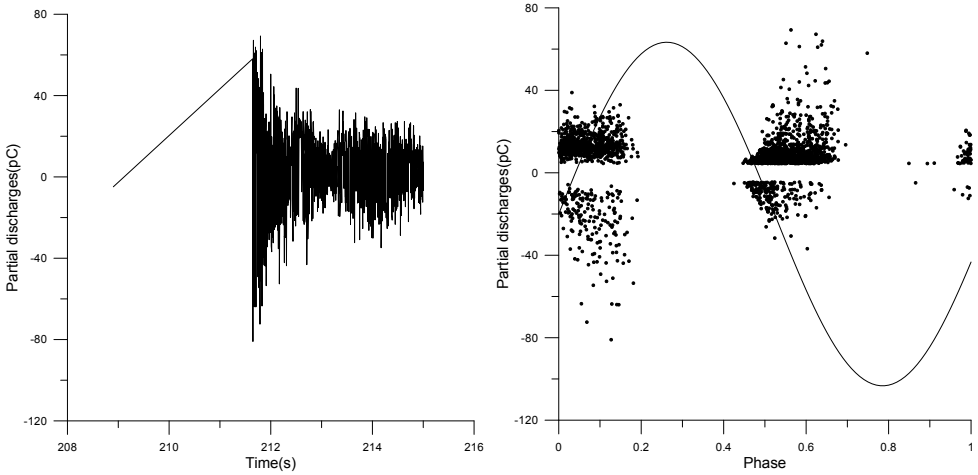

(c) Partial discharges as a function of time around the time of the expansion.

(d) The relation between each PD and the phase of the AC voltage.

Figure 4.4: The details of the expansion of the right droplet in the second D3_2 experiment.

When a droplet was left to dry on the surface, some of the water diffused into the sample. The water that diffused into the surface affected the results of the PD test by lowering the inception voltage. The droplet also expanded earlier, but was smaller than the expansion observed for a water droplet on a dry surface.

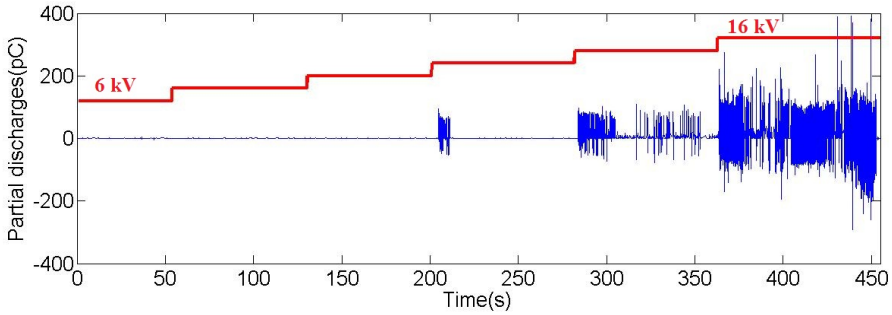

Figure 4.5: Time dependence of the PDs for a water droplet placed on a moist surface. The red line represents the voltage levels used in the experiments. The voltage starts at 6 kV and increases by 2 kV in every step until it reaches 16 kV.

When multiple small droplets were spread over the entire surface in a random pattern, the PD situation became very unpredictable. This can be seen from the large difference in inception voltage in the two situations. The reason for this large difference, is due to the difference in size and congestion of the droplets, see figure 4.6.

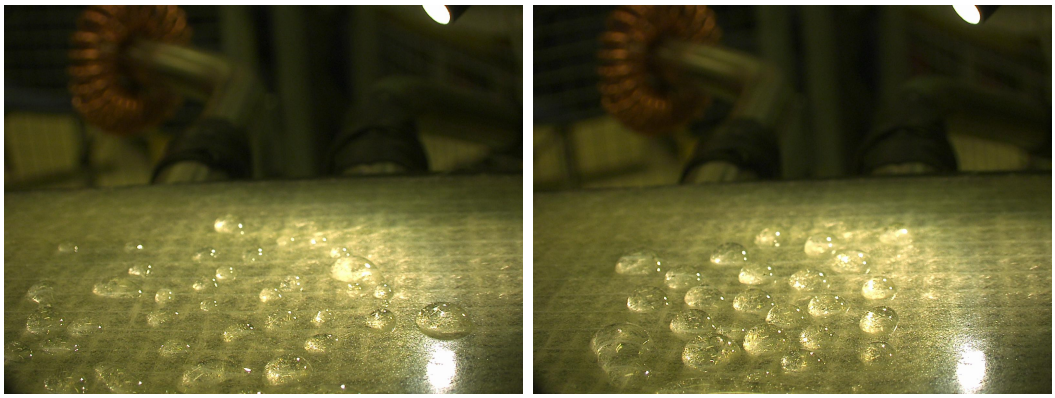

(a) 1st multiple droplet setup (b) 2nd multiple droplet setup

Figure 4.6: The two droplet setups used in the multiple droplet testing.

The second test had larger and more closely placed droplets and therefore a lower inception voltage.

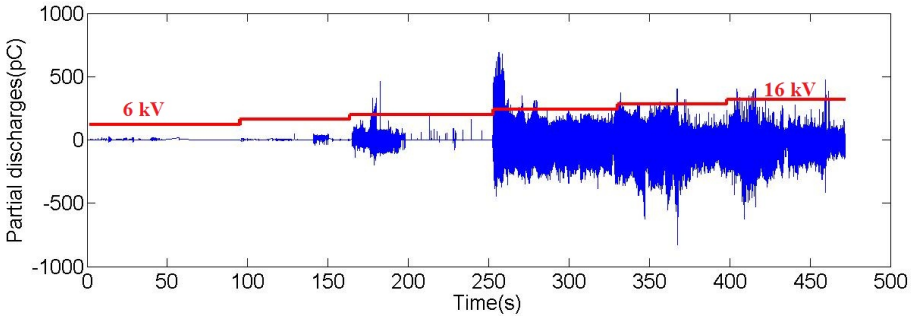

Figure 4.7: Time dependence of the PDs for the second multiple droplet test. The red line represents the voltage levels used in the experiments. The voltage starts at 6 kV and increases by 2 kV in every step until it reaches 16 kV.

There were some very small discharges at the 6 and 8 kV and also some droplet expansion of the more central droplets. When the voltage was raised to 10 kV the larger droplets started to tremble and significant PDs were observed. It was not until the voltage was raised to 12 kV that significant PDs and trembling of droplet surface were observed for the majority of the droplets.

4.1.2 Simulations

For all the experiments done with deionized water simulations were preformed. The distances between the drops in the multiple drop experiments varied slightly due to the difficulty in placing them in exactly the same position each time. Therefore two simulations were conducted here with the exact sizes and distances observed in the experiments. This meant that the situations with more than one droplets, were not completely symmetrical. The simulations were done with the voltage set to 16 kV. The voltage level only influenced the size of the field, not the shape. Therefore it was sufficient to conduct the simulations at only one voltage level.

The simulations where conducted in order to investigate the size and location of the greatest field enhancement. As expected, based on the theory, the water drops significantly increased the electric stress in their immediate vicinity [17].

Situation	Distance between drops (mm), left to right	Greatest E-Field enhancement
D1 100 µL		7
D1 50 µL		6.1
D2_1 1st	26	3.4
D2_1 2nd	24	3.5
D2_2 1st	12	5.8
D2_2 2nd	12	5.7
D2_3 1st	2	7.9
D2_3 2nd	0.9	10.8
D3_1	5.1 and 6	6.9
D3_2 1st	3 and 0.7	10.8
D3_2 2nd	2 and 1	11.2
D4 1st	0.76, 1 and 2.7	16
D4 2nd	1.48, 3.39 and 2.51	8.7
D5 1st	0.83, 1, 0.42 and 1	11.7
D5 2nd	2, 0.77, 3 and 1	9.6

Table 4.2: The distances between the droplets and the greatest electric field enhancement observed.

In order to investigate the quality of these COMSOL simulations the increase in field strength caused by one droplet was compared to the value expected from the approach used by Moukengué Imano et al. There was a difference in the two setups. Moukengué Imano et al placed the electrodes on the side of the insulation material. In this thesis work the electrodes were placed underneath. This difference in setup led to a difference in electric field at the edge of the droplet. In order to investigate this difference the field strength at the droplet edge was calculated with both eq (2.85) and with a modified version. In the modified version the U/d part was exchanged with the field strength obtained from COMSOL when there was no droplet on the surface. The field enhancement obtained straight from COMSOL was very similar to that obtained using the modified version of the approach developed by Moukengué Imano et al, see table 4.3.

$E_0 = U/d$(V/m)	E_0 given by COMSOL (V/m)	COMSOL simulation (V/m)
$7.12 \cdot 10^6$	$4.66 \cdot 10^6$	$4.32 \cdot 10^6$

Table 4.3: The electric field value at the tip of the droplet in the different methods used.

For the two cases with one droplet the field was symmetric. In the cases with two droplets the largest enhancement was at the left edge of the right droplet. In the cases with more then two droplets the largest enhancement was located in the smallest gap. The field situations for no droplet, one droplet and three droplets are shown in figures 4.8, 4.9 and 4.10 respectively.

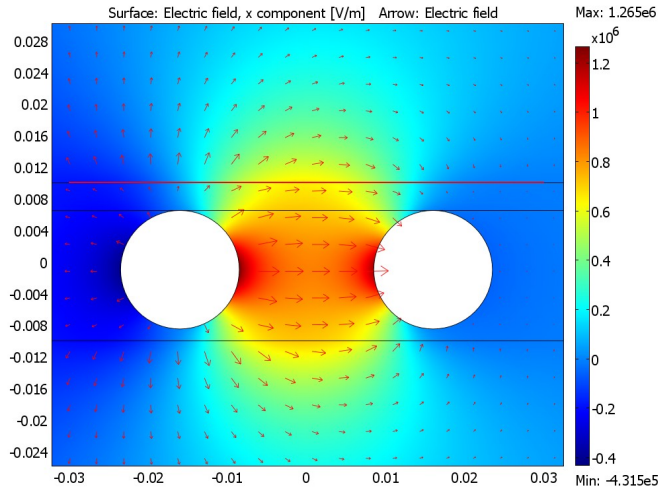

(a)

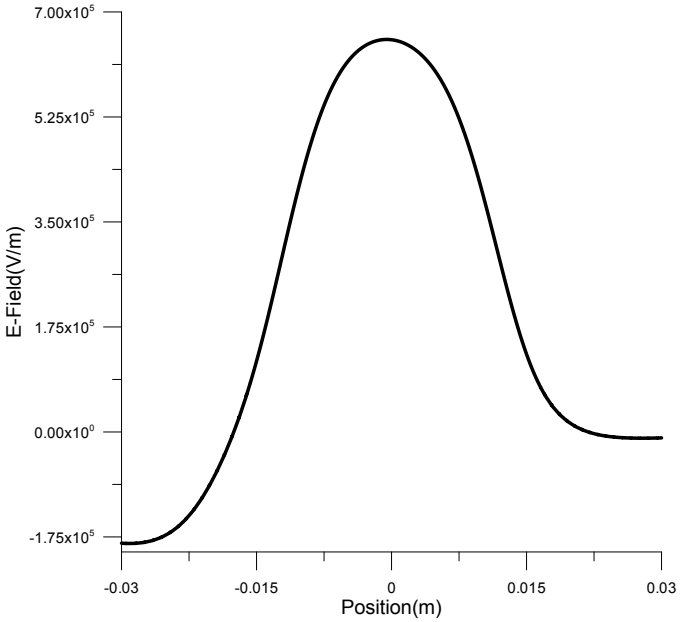

(b)

Figure 4.8: Electric field in the x-direction, when there is no droplet on the surface The red line seen in (a), shows where the data used in the graph in (b) was taken from

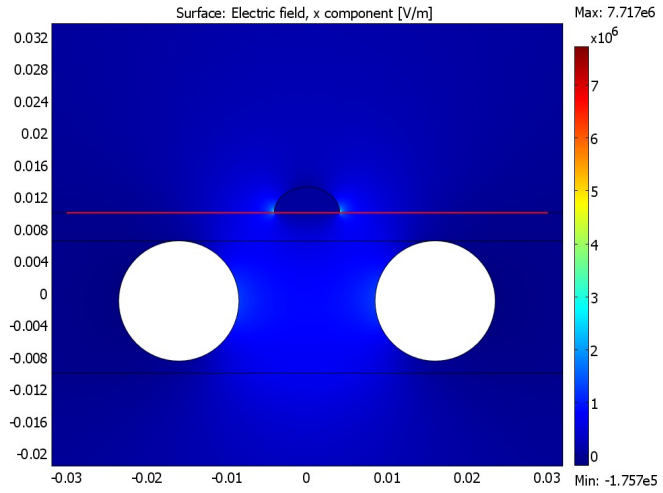

(a)

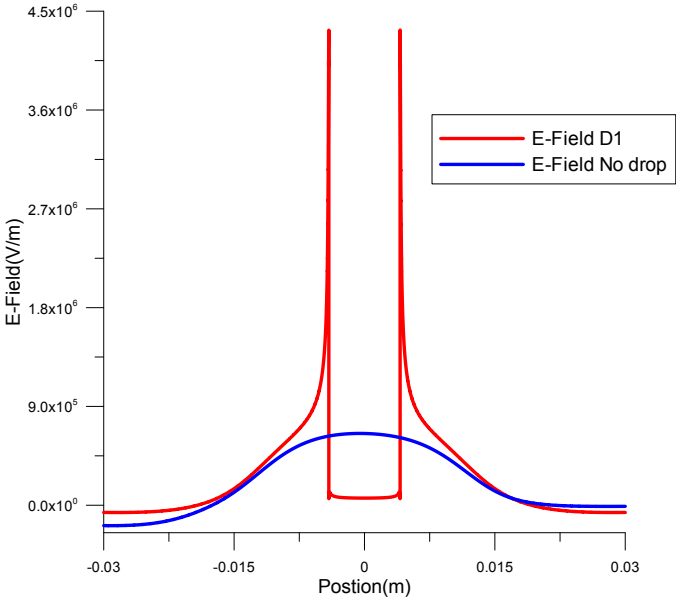

(b)

Figure 4.9: Electric field in the x-direction, when there is one droplet on the surface. The red line seen in (a), shows where the data used in the graph in (b) was taken from. The field situation on the surface when there is no droplet has been added as a reference.

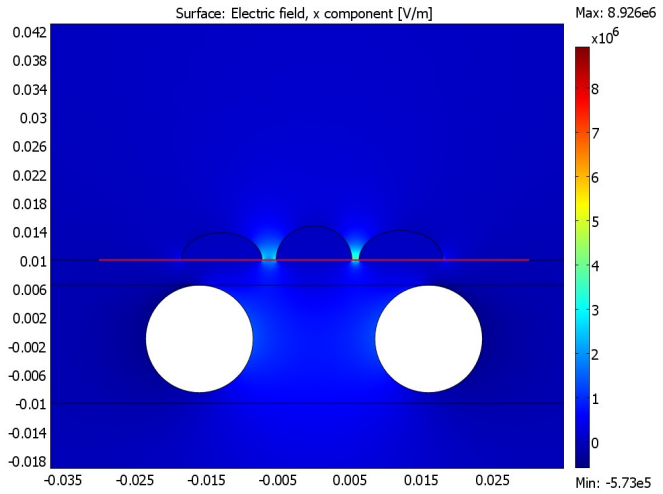

(a)

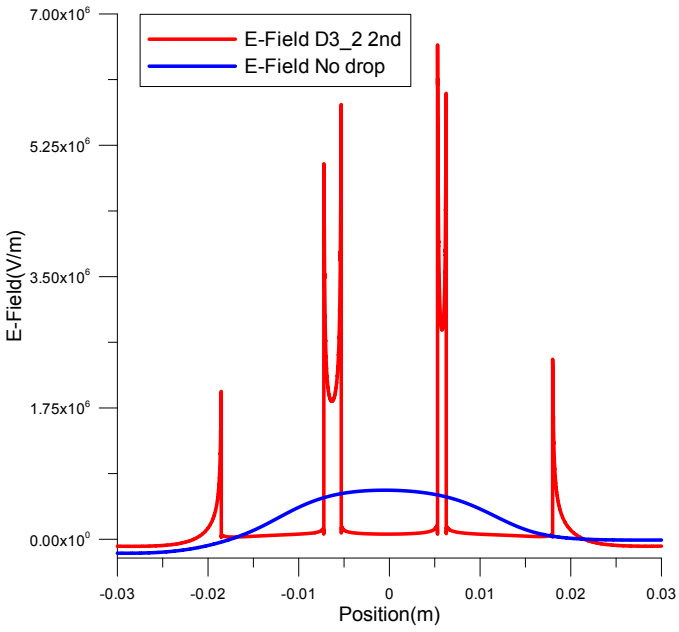

(b)

Figure 4.10: Electric field in the x-direction, when there are three droplets on the surface. The red line seen in (a), shows where the data used in the graph in (b) was taken from.

4.2 Salt water samples

4.2.1 Experiments

The difference between the water deionized water droplets and the artificial salt water droplets was the conductivity. Danikas et al had noted that an increase in the droplet conductivity would lead to a decrease in the inception voltage level [14]. The inception voltages observed in the experiments are listed in the following table. For the salt water tests only one, three droplets and multiple small droplets were studied.

Situation	Inception voltage level (kV)
D0	No discharges
D1 100 µL 1st	14
D1 100 µL 2nd	16
D3_2 1st	8
D3_2 2nd	12
D3_2 3rd	8
D3_2 after drying 1st	8
D3_2 after drying 2nd	10
Multiple droplets 1st	10
Multiple droplets after drying 2nd	6
Multiple droplets after drying 3rd	6

Table 4.4: The inception voltage in all the situations tested. In the multiple droplet drying test the PDs were small and variable at 6 kV.

The general behavior of the droplets was very similar in the deionized and salt water experiments, but for the D1 tests the elongation of the droplet happened more gradually. Therefore there was no clear point of elongation to study for this case, so the entire experiment was studied as if it were one expansion. In the D3_2 case there was a clear elongation of the right drop. The elongation development is shown in figure 4.11. The procedure for determining the width of the droplets and the changes in voltage levels was the same for the salt water samples as for the deionized water samples. The elongation and PDs detected in the two situations are shown in the following graphs.

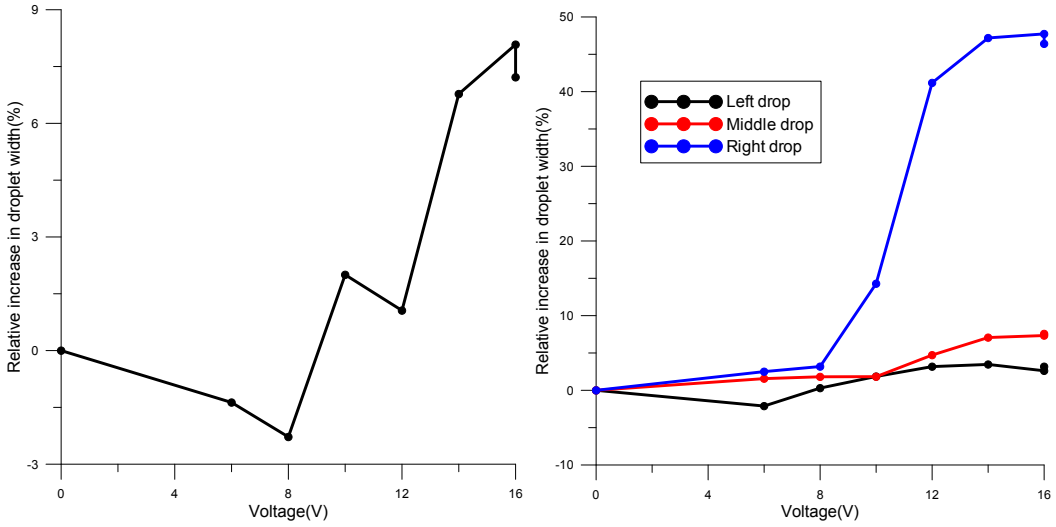

(a) D1 (b) D3_2

Figure 4.11: Change in droplet width, in % of the start width, as a function of voltage, for salt water drops on a dry surface.

There was no clear difference in PD behavior when three droplets were placed in the same places as dried up droplets. For the multiple droplets the partial discharges started earlier when there was salt on the surface. In the two cases studied there were droplets placed both in the same places as previous tests and in new locations. Therefore the salt on the surface was a more significant factor in these cases then in the three droplet cases.

In the third multiple droplet study, there are some small discharges at 6 and 8 kV. In the first case the discharges does not start until the voltage is raised to 8 kV.

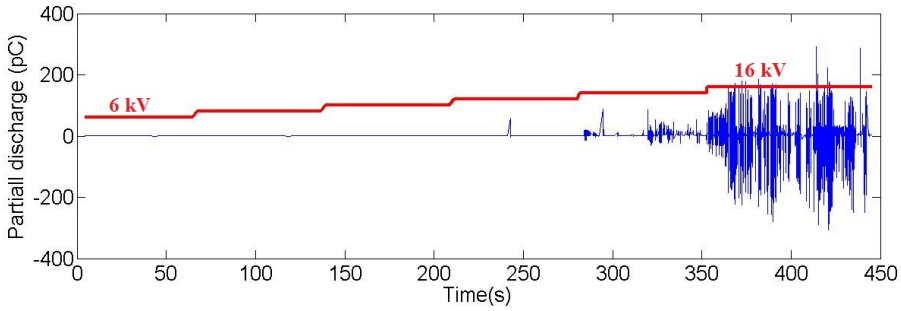

(a) D1

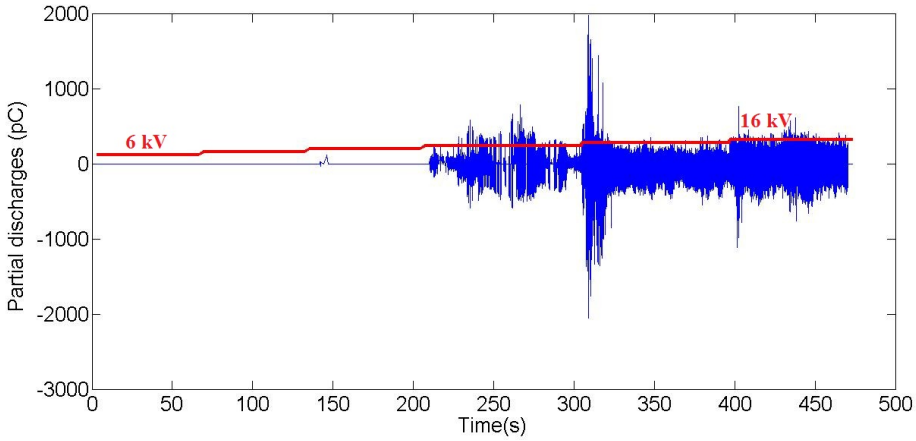

(b) D3_2

Figure 4.12: Time dependence of the PDs for one and tree salt water drops on a dry surface. The red line represents the voltage levels used in the experiments.

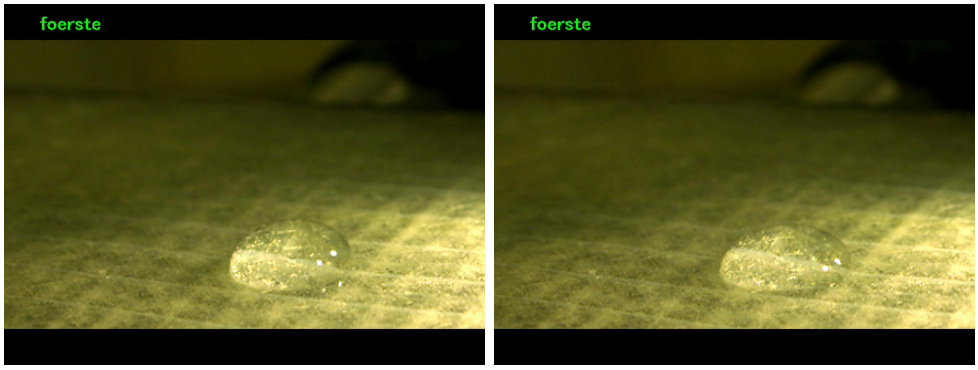

(a) Droplet at the start of the experiment w=8.5 mm

(b) Droplet at the end of the experiment w=8.5 mm

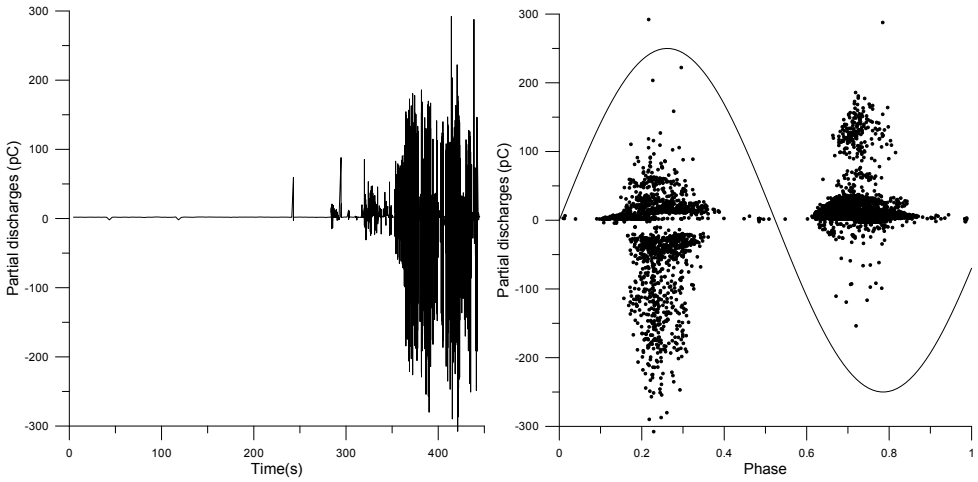

(c) Partial discharges as a function of time around the time of the expansion.

(d) The relation between each PD and the phase of the AC voltage.

Figure 4.13: The details of the expansion of the a salt water droplet on the sample surface. The PD event shown in the figure are from when the first significant PDs were detected.

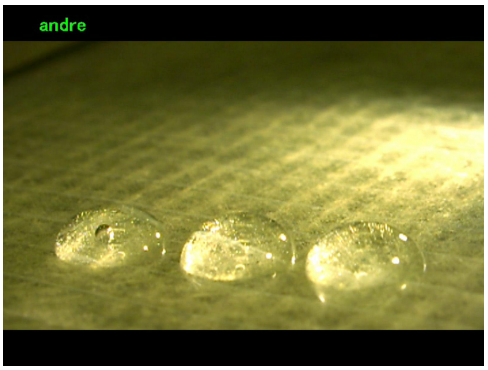

(a) Droplets before the expansion. w_l=8.5 mm, w_m=8.5 mm and w_r=8.5 mm

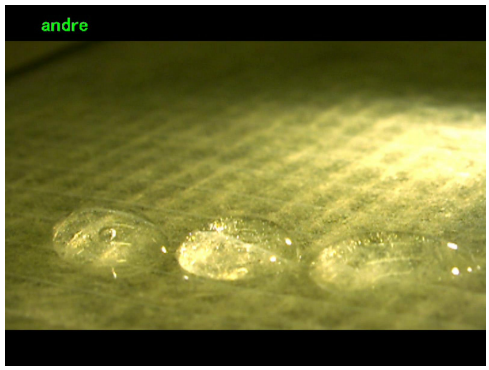

(b) Droplets right after the expansion. w_l=8.5 mm, w_m=8.5 mm and w_r=8.5 mm

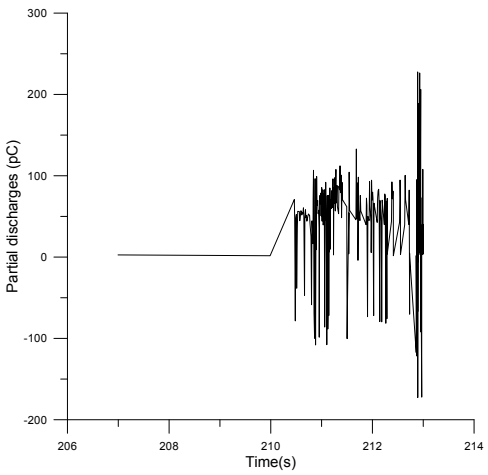

(c) Partial discharges as a function of time around the time of the expansion.

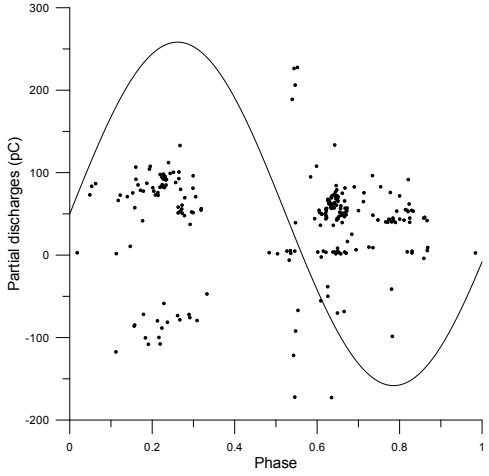

(d) The relation between each PD and the phase of the AC voltage.

Figure 4.14: The details of the expansion of the right droplet in the second D3_2 salt water experiment.

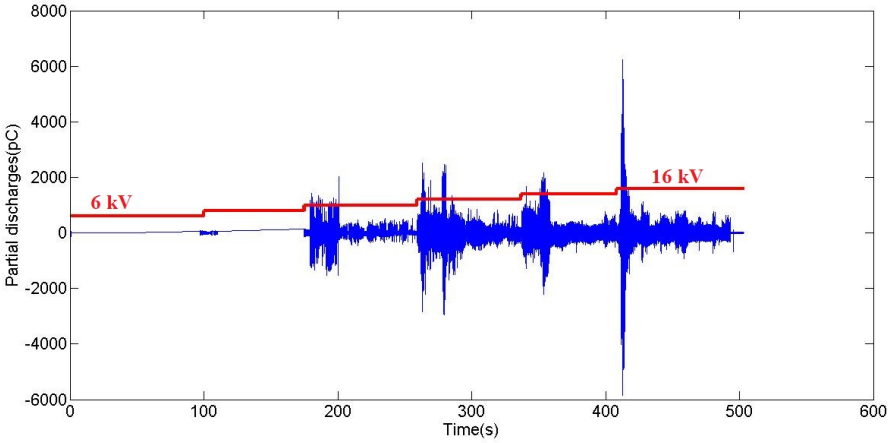

(a) 1st multiple droplet setup

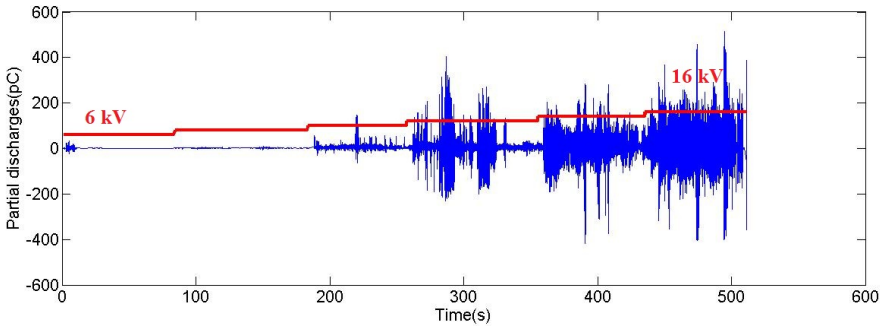

(b) 3rd multiple droplet setup

Figure 4.15: Time dependence of the PDs for multiple salt water drops on a dry surface. The red line represents the voltage levels used in the experiments.

4.2.2 Simulations

The simulation model used in this thesis work, did not consider the conductivity of the droplets when calculating the field. This meant that the field calculations for the salt water drops only differed from the deionized drops by relative the position of the drops. When salt drops were left to dry on the surface, they created a mold for new drops to be placed in. This meant that the droplet orientation for the dried droplets was significantly different and this again led to a different field.

Situation	Distance between drops (mm), left to right	Greatest E-Field enhancement
D1		7
D3_2 1st	0.17 and 2.6	17.5
D3_2 2nd	1.2 and 0.9	11.6
D3_2 before drying	0.6 and 1	12.6
D3_2 after drying	0.6	13.6

Table 4.5: The distances between the droplets and the greatest electric field enhancement recorded for the salt water experiments.

4.3 Oil saturated sample

4.3.1 Experiments

For the tests with oil saturated sample only one and three droplet setups were tested. Both setups were tested with deionized and salt water. The presence of oil had a clear effect on both the PD situation and the droplet behavior. The PDs started earlier and were larger. The droplets expanded more and there were even cases of droplets separating into two or more parts.

Situation	Inception voltage level (kV)
D0	No discharges
D1100 µL 1st	12
D1 100 µL 2nd	12
D3_2 1st	8
D3_2 2nd	6
D1100 µL salt 1st	10
D1 100 µL salt 2nd	10
D3_2 salt 1st	6
D3_2 salt 2nd	8

Table 4.6: The inception voltage in all the situations tested for the oil saturated samples.

The second test of the D3_2 setup resulted in a merging of the left and middle droplet immediately after the voltage was set to 6 kV. This is shown in figure 4.16b. The plots showing the change in relative droplet width for the left and middle drops, used the initial value of each of the separate drops as the starting point. The merged plot used the sum of width of the two drops as a starting point.

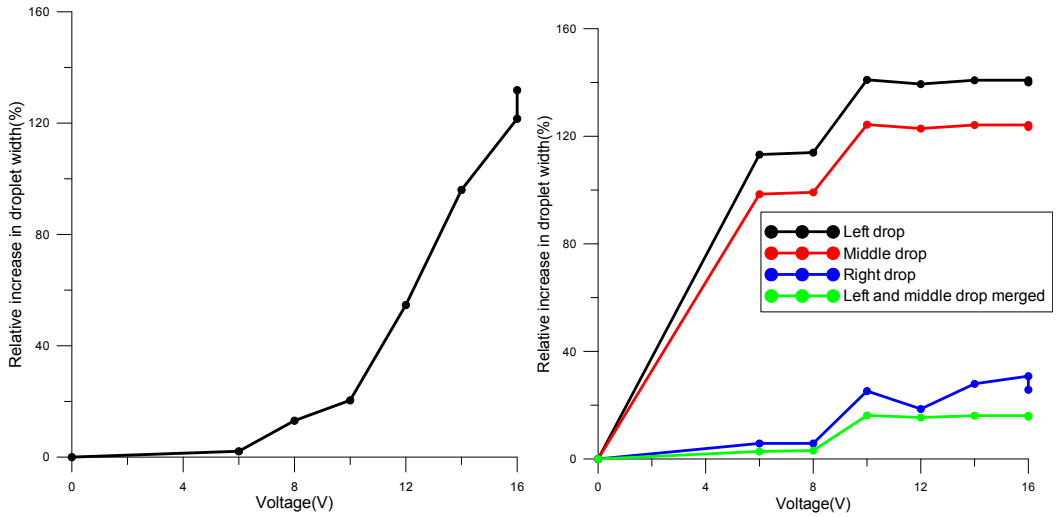

(a) D1 (b) D3_2

Figure 4.16: The time dependence of the PDs for one and three deionized water droplets on an oil saturated sample. The red line represents the voltage levels used in the experiments.

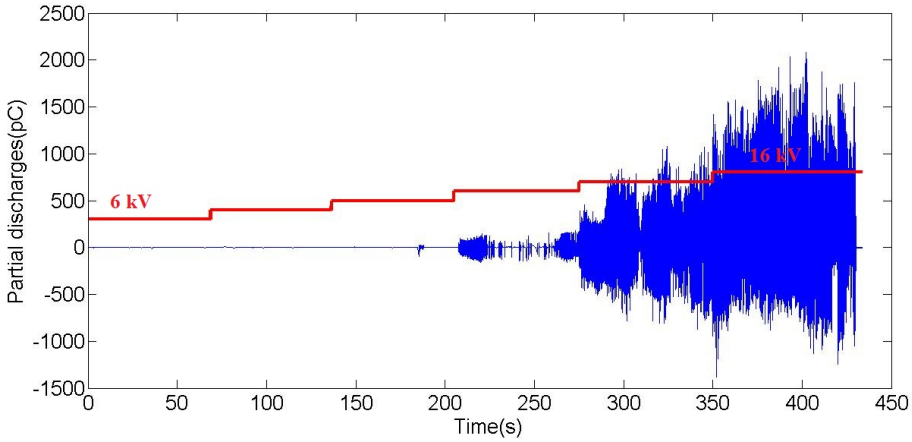

(a) D1

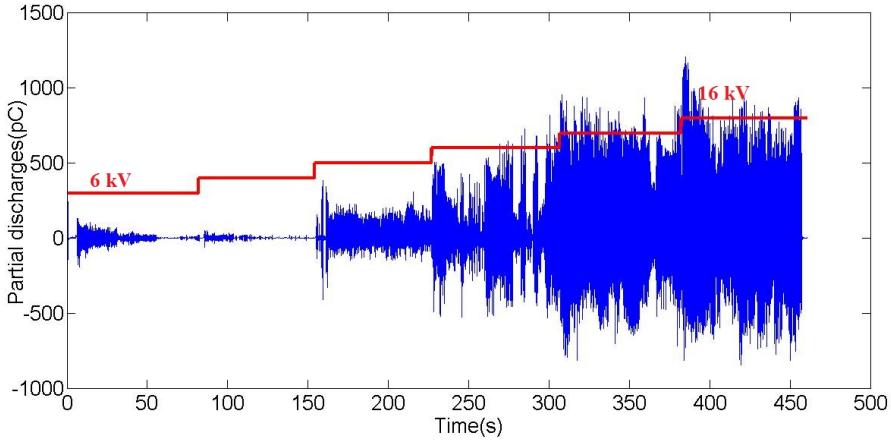

(b) D3_2

Figure 4.17: Change in droplet width, in % of the start width, as a function of voltage, for salt water drops on a dry surface.

From figure 4.17 it is clear that the PDs recorded in the tests with an oil saturated sample, is much larger than those recorded in the tests with a dry sample. The number of partial discharges recorded was also much higher than for the dry samples. Because of this the length of the PD samples selected for closer study were much smaller.

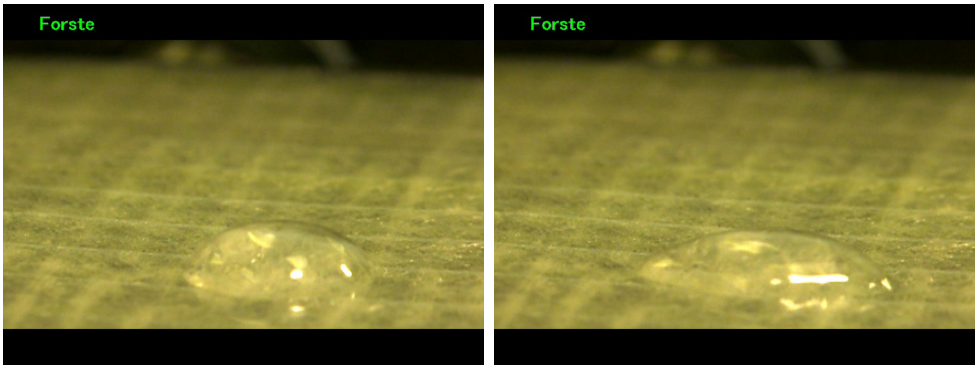

(a) Droplet before the expansion. w=9.73 mm

(b) Droplet after the expansion. w=12.5 mm

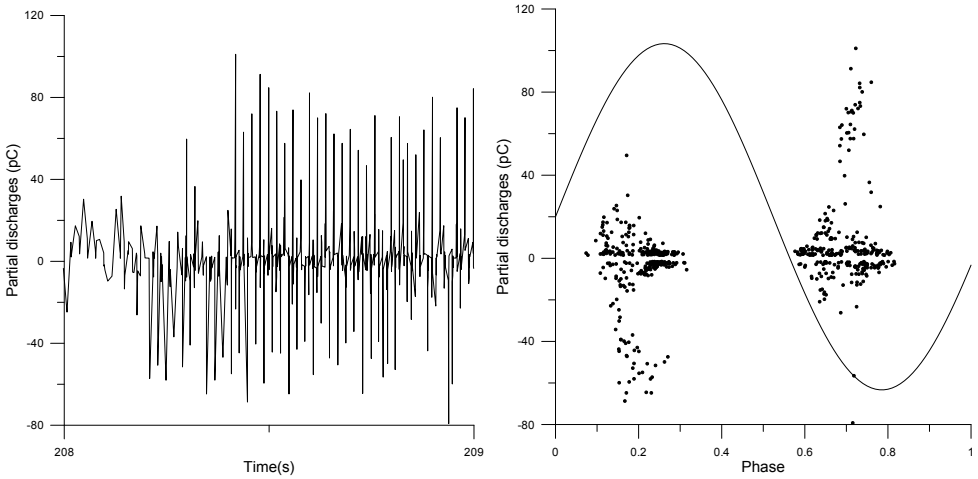

(c) Partial discharges as a function of time around the time of the expansion.

(d) The relation between each PD and the phase of the AC voltage.

Figure 4.18: The details of the expansion for a deionized water droplet on an oil saturated surface.

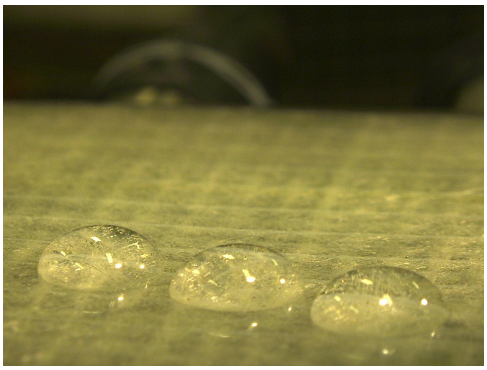

(a) Droplets before the expansion. w_l=8.8 mm, w_m=9.44 mm and w_r=9.79 mm

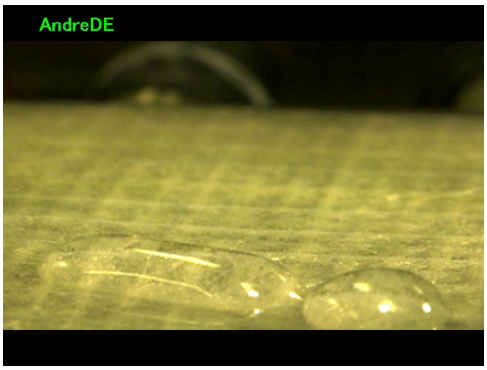

(b) Droplets right after the expansion. w_l=18.74 mm and w_r=10.36 mm

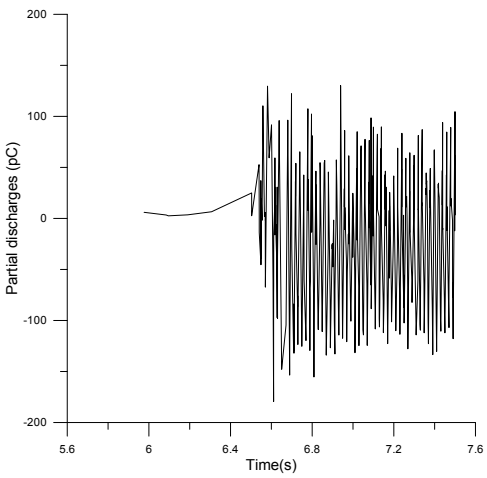

(c) Partial discharges as a function of time around the time of the expansion.

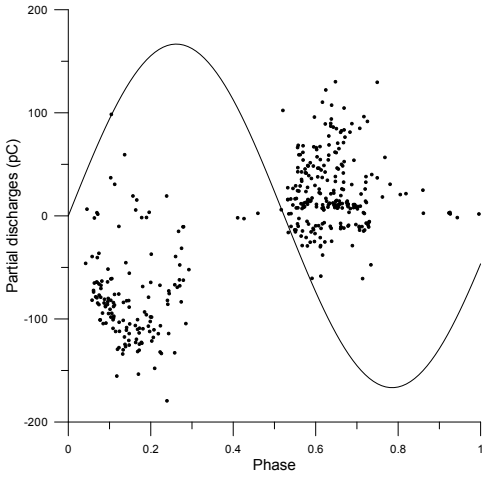

(d) The relation between each PD and the phase of the AC voltage.

Figure 4.19: The details of the expansion and merging for three deionized water droplets on an oil filed sample.

When salt water drops were placed on an oil saturated surface the size of the expansions increased. The first single droplet placed in the middle of the two electrodes expanded to more then twice its original size before splitting twice. The first splitting occurred when the voltage was raised to 14 kV, and the second about 43 s after the voltage had been raised to 16 kV. This is shown in figure A.2. In order to show that the droplet covered a larger area

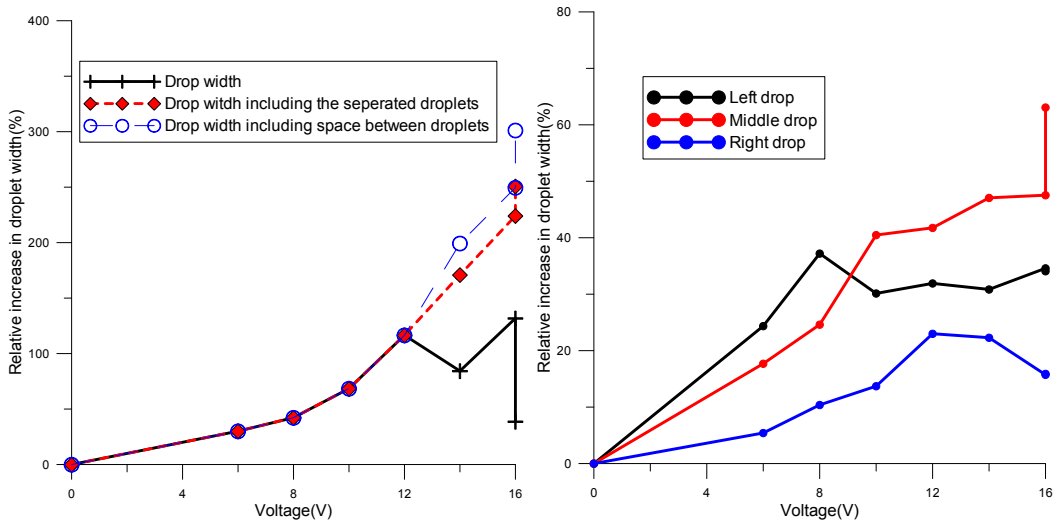

(a) D1 (b) D3_2

Figure 4.20: This figure shows the time dependence of the PDs for the entire test. The red line represents the voltage levels used in the experiments.

after the splitting, extra width plots where included in 4.20a. The two extra plots included the widths of the new drops and the distances between them.

The setup with three droplets did not experience the same splitting of droplets that was observed in the setup with one droplet, but it did have an instant expansion when the voltage was set to 6 kV, and the highest number of discharges of all the setups.

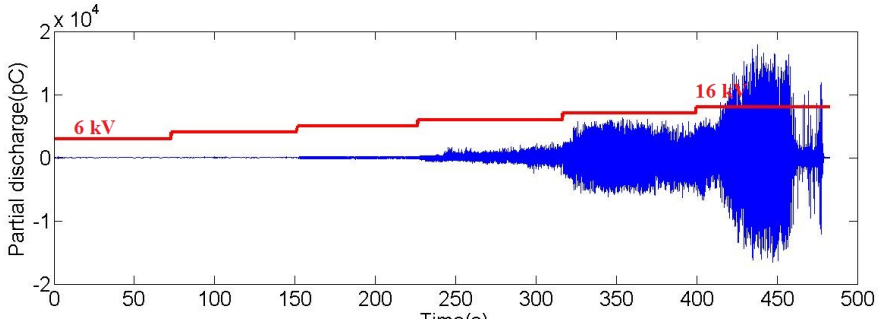

(a) D1

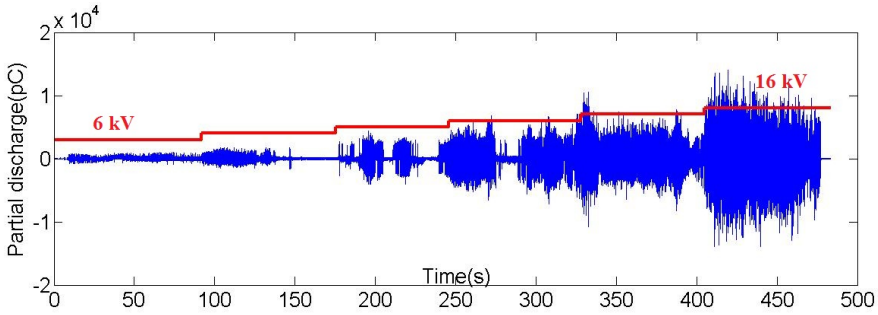

(b) D3_2

Figure 4.21: This figure shows the time dependence of the PDs for the entire test. The red line represents the voltage levels used in the experiments.

The experiment with one salt droplet on the oil saturated surface had two significant expansions before the first PDs were detected. Therefore the expansion that was studied was the expansion that occurred when the voltage was raised from 8-10 kV. Due to the incredible amount of PDs detected in these experiments, 9 000 000 for D1 and 19 000 000 for 3D_2, the time intervals used to study the expansions were even smaller.

(a) Droplet before expansion. w=10.6 mm

(b) Droplet after expansion. w=12.5 mm

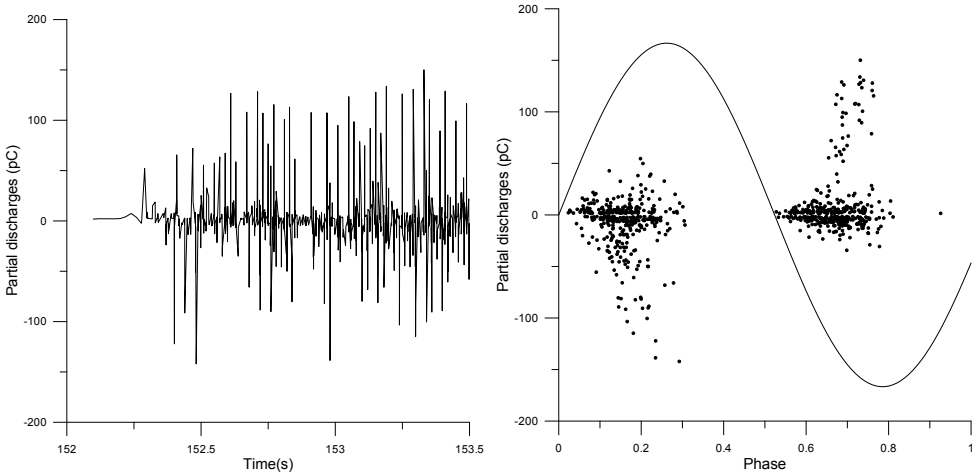

(c) Partial discharges as a function of time around the time of the expansion.

(d) The relation between each PD and the phase of the AC voltage.

Figure 4.22: The details of the expansion of one salt water droplet on an oil saturated surface.

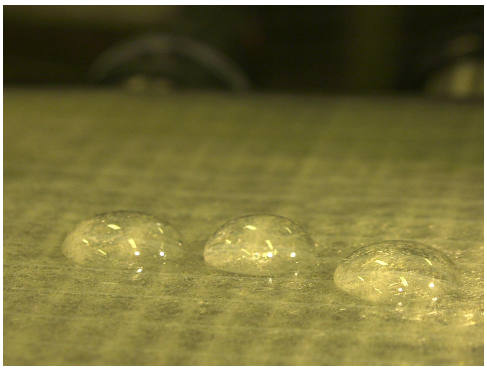

(a) Droplets before the expansion. w_l=8.31 mm, w_m=7.39 mm and w_r=8.3 mm

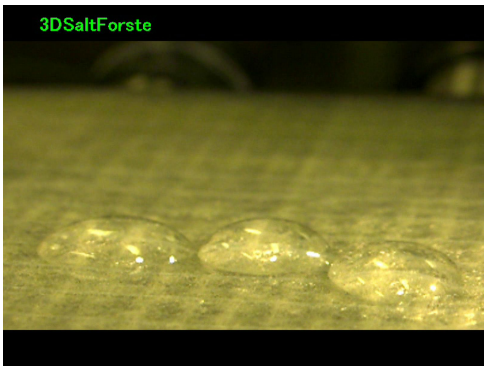

(b) Droplets right after the expansion. w_l=10.34 mm, w_m=8.7 mm and w_r=8.75 mm

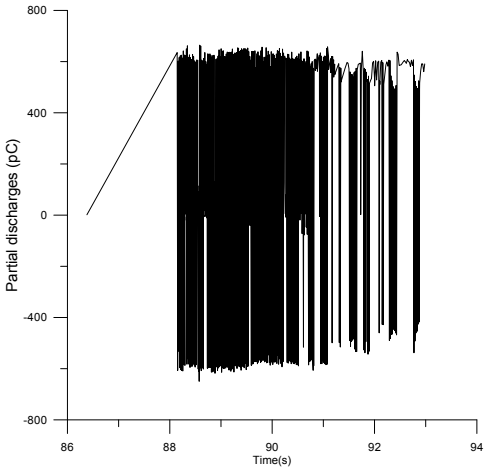

(c) Partial discharges as a function of time around the time of the expansion.

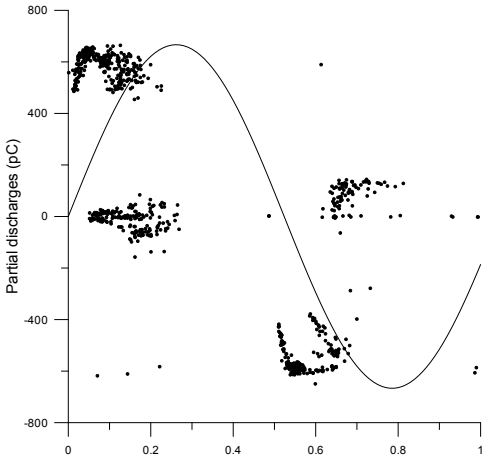

(d) The relation between each PD and the phase of the AC voltage.

Figure 4.23: The details of the expansion of all three droplets in the second D3_2 experiment for salt water drops on an oil saturated sample.

4.3.2 Simulations

The electrical difference between the oil saturated sample and the dry sample was a change in permittivity. When the sample was completely saturated with oil, the permittivity increased from 3.6 to 4.9. This change in permittivity had only a small effect on the field on the surface of the sample. The changes in field enhancement caused by the droplets was also very small, about 7% for one 100 µL droplet.

Situation	Distance between drops (mm), left to right	Greatest E-Field enhancement
D1		6.5
D3_2 deionized water	1.4 and 1.7	10.5
D3_2 salt water	1 and 1.7	10.4

Table 4.7: The distances between the droplets and the greatest field enhancements detected.

The shape of the field was similar to that observed for dry samples.

4.4 Liquid-Contaminant Inclined-Plane Tracking and Erosion test

4.4.1 Surface roughness

The effect of the erosion test was determined by measuring the difference in the surface topography before and after the test. For the test sample with no oil present there was no significant difference in the surface topography when the current was set to about 6 kV. When the voltage was raised to 10 kV, the topography was noticeably different. The largest and clearest difference was observed in the measurement conducted over the high voltage electrode and the smallest difference was observed in the middle of the electrodes.

Based on the data from the droplet tests the oil saturated sample should experience a lot of PDs when the voltage was set to 10 kV. Due to time constraints it was only possible to run the erosion test on the oil saturated sample for one week. In this experiment salt water flowed down the surface in just two places. During this test there were some problems with the water flow around the 20 000 µm mark. The flow would occasionally stop in the middle of a test without any outside action. This meant that the oil saturated sample only had one good water flow. However, there appears to have been a a definite erosion of the surface around this dripping line.

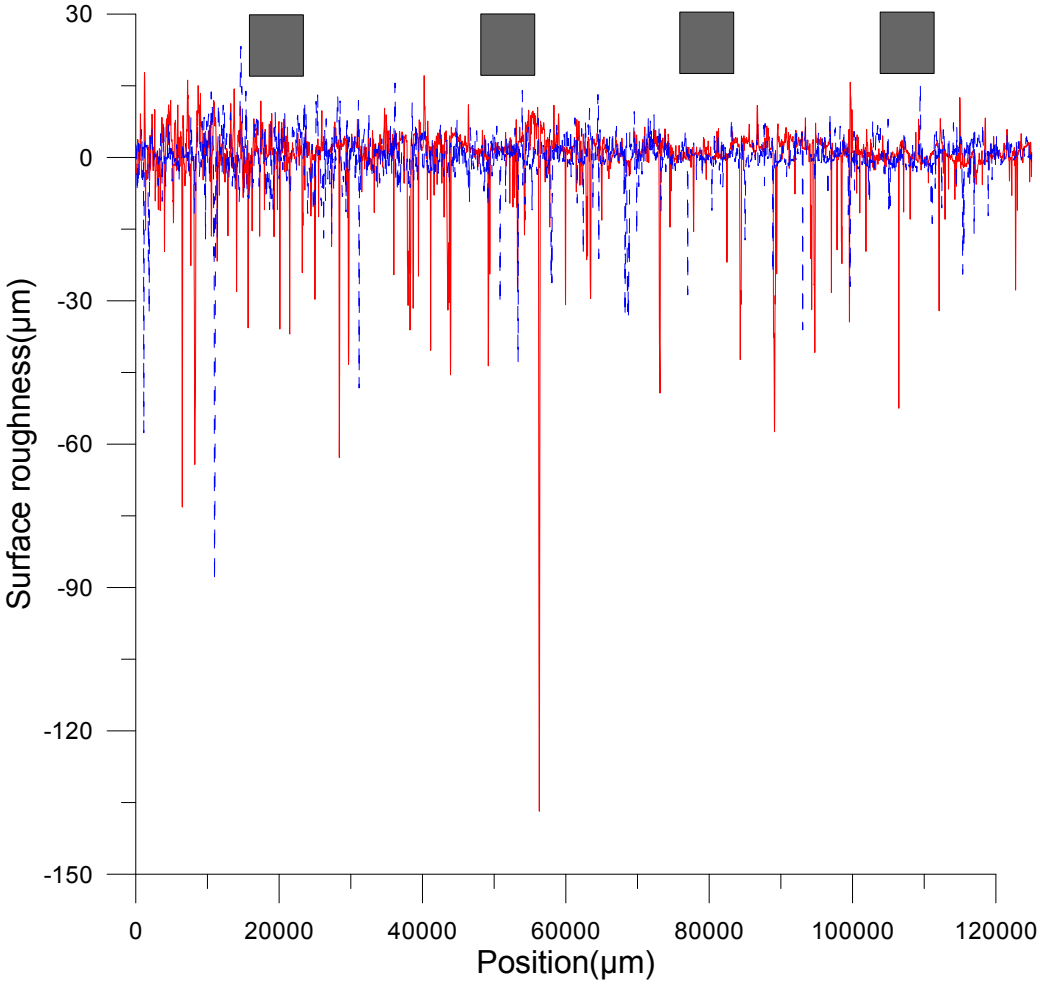

Figure 4.24: The difference in surface roughness before and after the salt water had been applied for two weeks. The blue dotted line represents the surface at the beginning and the red line represents the surface after a week of testing at 10 kV. The gray squares represents the positions were the water flowed.

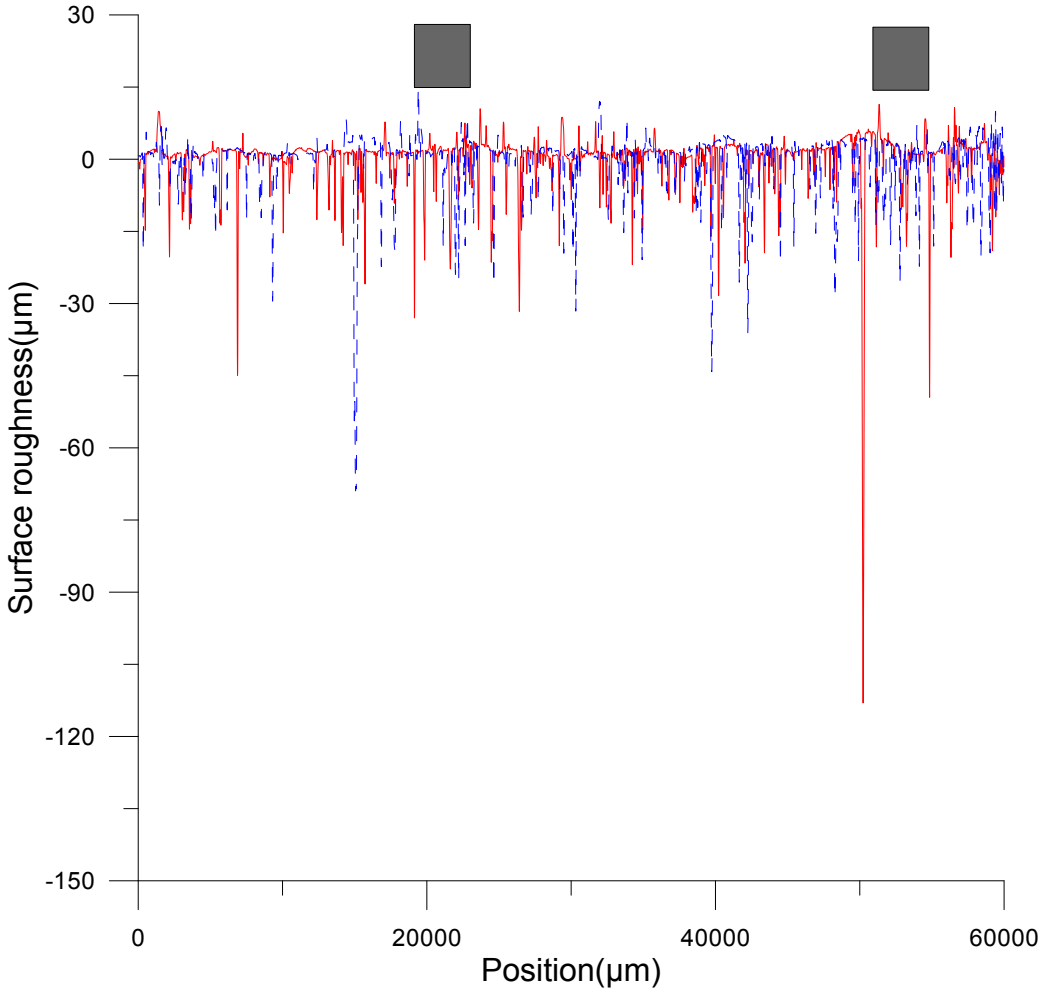

Figure 4.25: The difference in surface roughness before and after the salt water had been applied for one week. The blue dotted line represents the surface at the beginning and the red line represents the surface after a week of testing at 10 kV. The gray squares represents the positions were the water flowed.

Chapter 5

Discussion

5.1 Deionized water droplets

Table 4.1 shows that the inception voltage decreases when there are more droplets involved. The distances between the droplets and where the droplets were placed, also effects the inception voltage. When the droplets are placed above the two electrodes, e.g. in situation D2_1, there are no discharges. Placing three drops close together decreases the inception voltage compared to one droplet alone in the middle. Increasing the number of droplets further decreases the inception voltage. Decreasing the droplet volume leads to an increase in the inception voltage, but the effect of multiple droplets is larger than the effect of droplet size. These results are backed up by the simulations, table 4.2. Danikas et al came to the same conclusions in their work as well [14]. This gives credibility to the results obtained in this thesis work. The difference in inception voltage between the two measurements for each of the multiple droplet setups, was due to the differences in positioning of the droplets. A good example of this was the case with five droplets. The shortest distance between two droplets in the first case was only 0.42 mm. The second case had a minimum of 0.77 mm between its droplets. The differences in the field enhancements and inception voltage reflects this. The first case has both higher field enhancement and lower inception voltage. The electric fields obtained in the simulations were similar in shape and size to simulations conducted by e.g. Moukengué Imano et al and can therefore be

assumed to be quite accurate.

Significant discharges were first detected around the time of the first large expansion. When there were more droplets, larger field enhancement, the size of the discharges increased. In most of the cases studied, the expansion occurred almost at the same time as the increase in the voltage level. Significant partial discharges were also discovered when the voltages was increased, usually right after an expansion. Both partial discharges and droplet expansion, depended on the size of the electric field. Both activities started when the field was raised beyond a given level. The voltage increased by 2 kV at every step in the measurements. This meant that the field became significantly larger as well. When the droplet expanded, the field enhancement became larger due to the increase in width and sharpness of the contact angle. [5] [18] Hence the droplet system was a positive feedback system. It was this major increase in electric stress that caused the partial discharges recorded in the experiments.

The video recordings made with the microscope, showed the expansion of the droplets very clearly. The expansions were just like those described by S. Keim et al [7]. When the expansion occurred, the droplet was visibly dragged wider. The process started with a slow gliding of the edge and ended with a sudden burst. When partial discharges, larger than about 50 pC, were recorded with the Mtronix equipment, the surface of the droplet visibly trembled. This trembling corresponds to the oscillation behavior that S. Keim et al observed [7]. There was no high speed camera used in this work, so the exact oscillation period of the surface trembling could not be determined.

When the surface underneath the droplet had absorbed some water the inception voltage became smaller. The reason for this could be the increase in moisture around the droplet. S. Feier-Iova and V. Hinrichsen discovered that the inception voltage level dropped with increasing air moisture [10]. A thorough investigation of a water saturated sample is necessary to obtain conclusive information about this phenomena.

5.2 Salt water drops

Increasing the conductivity of the droplets resulted in a lower inception voltage, when more than one droplet was present. One salt water drop behaved very differently than one deionized water droplet, when placed on the surface. There was no large and sudden expansion of the droplet width. When three droplets were placed close together the situation was more like that observed for deionized water. When the shortest distance between the droplets was about the same the field enhancement and inception voltage were similar. The salt water drops had the same shape and contact angle as the deionized water droplets, so the surface tension did not change significantly.

When salt water droplets were placed in the molds left behind by the evaporation of other salt water drops no expansion was detected. The salt water solutions that were used in these measurements were not saturated with salt. When the new droplets were placed in the salt rings left behind by the old drops, the salt on the surface was most likely absorbed into the salt water droplets. These new droplets had the same shape as the droplets at the end of the last experiment. The droplets from the first test were expanded as much as possible by the electric field. The new droplets were therefore already expanded when the measurement started.

In the multiple droplet tests the drops were not placed in the exact same position each time. In these cases the inception voltage was lowered after the drying. The salt on the surface may have led to an increase in the surface conductivity, which in turn increased the chances of partial discharges.

5.3 Oil saturated samples

When the sample was saturated with oil, the inception voltage levels dropped. The expansions also occurred at lower voltages. The size of the expansion was also much larger, especially in the cases with only one droplet. When the voltage was raised to 16 kV, the droplet width was more than twice what it had been at the start. For the salt water drop this doubling of the width occurred at 12 kV. When the voltage was increased further the droplet

broke apart. In all, but one of the three droplet cases with an oil saturated samples studied here, there was merging of one or more droplets. The distances between the droplets were similar to those in the dry tests, where no merging was observed. The contact angle did not change significantly when the sample was saturated with oil. This means that the difference in surface tension between the oil saturated situations and the dry situations was small.

The presence of oil inside the sample had a very small effect on the permittivity of the sample, an increase from 3.6 to 4.9. This meant that the size of the electric field on the surface of the sample changed very little. The field enhancements were therefore about the same for droplets a oil saturated surface as for those on dry a dry surface. This surprising behavior was discussed with Gunnar Berg at SINTEF and two different hypotheses were produced.

5.3.1 Decreased surface roughness due to oil diffusion

The surface of the samples used in the experiments were not completely even. After oil had diffused into the surface, it is possible that it caused an evening out of the surface. The oil may have gathered in the small depressions on the surface or covered up elevated parts. This may have provided the droplet with fewer places to attach itself to the surface. This evening of the surface may have, along with the oil itself, lowered the friction coefficient of the surface. A lower friction coefficient would have made it easier for the droplet to move on the surface, and by extension, lowering the force required to expand a droplet. Comparing the surface roughness with and without oil lends some weight to this theory.

The Mitutoyo device showed both the peeks and cracks of the surface it measured. The surface of the oil saturated sample, figure 5.1a, has a lot fewer large peeks then the dry sample, figure 5.1b. This trend is observable in all the measurements taken of the two surfaces. A closer study is needed in order to obtain a definitive answer. The best approach would be to measure the roughness at the exact same place both before and after oil saturation. In order to investigate how oil diffusing onto the surface affected the surface roughness, a series of measurements should be conducted over time after the sample has been removed from the oil bath.

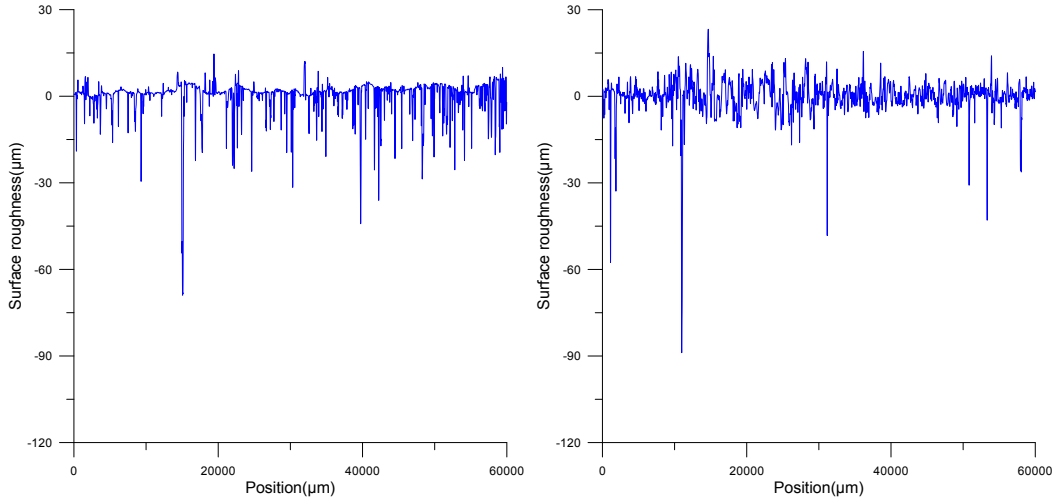

(a) Oil saturated sample (b) Dry sample

Figure 5.1: Surface roughness before high voltage was applied to the samples. Only half the length of the dry sample is used, in order to make the comparison of the two easier.

The change in friction between the droplet and the surface caused by the oil can be determined experimentally. One possible setup is to place a charged droplet on the surface between two electrodes and applying a DC voltage difference over the electrodes. The droplet can be charged by touching it directly with a low voltage electrode. When the droplet is charged it will move in a homogeneous electric field in the direction of the field, see figure 5.2.

By measuring how far the droplet moves on a dry and oil saturated sample the differences in the friction between the water droplet and the surface can be determined. A simpler setup would have been to place droplets on a vertical surface and observe how it moves down the surface.

Figure 5.2: Charged droplet in a DC field

5.3.2 Reduced electrostatic attraction due to increased surface conductivity

No material is a perfect insulator. There will always be some charge carriers that are free to move about the material. In a dielectric material the movement of charge is done by ions and electron hopping. Water is a polar molecule and in an electric field these molecules will align themselves in the direction of the field. Any charge neutral body placed in an electric field will behave as a dipole [19]. The main difference between materials is the speed of the dipole arrangement. Metals have an almost instantaneous reaction to electric fields, while in dielectric bodies the process takes time. In general the polarization of a material is much faster than the redistribution of charges caused by conduction in the material. Even dielectric materials have a limited conduction of charge. The time constant for the redistribution of charge, $\tau = \epsilon_0 \epsilon_r / \sigma$, is an important parameter in separating conductors from insulators. It is a measurement of how quickly the material recovers from

the effects of the electric field. This time constant is equivalent to the time constant of a capacitor, $\tau = RC$, where C is the capacitance and R is the resistance. This time constant determines the speed with which charges of in a dielectric placed in an electric field leaks away.

In the experiments preformed in this work the electric field provided by the electrodes caused an accumulation of charge at the surface. The dipoles in the water droplet were aligned by these charges, leading to an electric field over the surface. This field created an electric force between the droplet and the surface, keeping the droplet in place. According to Lundgaard and Berg et al oil has a much shorter relaxation time constant then a solid insulator, due to larger conductivity. They estimated a relaxation time constant for a solid insulation to be between $5.3 \cdot 10^3$ and $3.5 \cdot 10^5$ s [19]. Pure oil had a relaxation time constant between 27 and 177 s. This means that oil will lose its charge much faster than a soil insulator.

It is possible that when the oil diffused into the surface the relaxation time constant of the surface was lowered significantly. This would have lead to a decrease of the electric force between the droplet and the surface. This would again have lead to a smaller force keeping the droplet in place and thereby making it easier to move. This would explain why the droplets placed on an oil saturated sample expanded at lower voltage then those on a dry sample.

In order to determine whether there was a difference in surface conductivity between an oil saturated sample and a dry sample, new experiments would have to be conducted. In these experiments the samples would have to be exposed to high voltage for a given time. When the applied voltage was turned off, the voltage left behind in the sample would need to be measured over a large time span. The relaxation constant of the two situations could then be measured and compared. If the oil saturated sample had a significantly shorter relaxation time constant than the dry sample, then this might explain the differences observed in this thesis work.

5.4 Droplet expansion and breakup

If a spherical droplet is placed in an electric field the relation between the semi axis will theoretical change according to eqs (2.16) and (2.19) for a conductive and dielectric drop respectively. For the field strengths used in this work the changes are given in table 5.1.

Situation	a/b
Conductive drop	1.28
Dielectric drop	1.24

Table 5.1: Theoretical calculation of the change in the relationship between the two semi axis of a free water droplet in an electric field at 16 kV

The data in 5.1 was obtained by using the electric field calculated in the COMSOL simulations and the graphs shown in figures 2.2 and 2.3. The field strength was collected at 16 kV and represents the highest possible background field available during the experiments. The difference between the two are minimal and supports the assumption of regarding the drop as a conductive medium.

T.Schütte and S. Hornfeldt discovered a quantitative similarity between the behavior of a free droplet and a sessile droplet in an electric field [20]. The sessile droplets observed in this thesis work had a much greater elongation than the elongation expected for a free droplet. The sessile droplets had an increase in width of about 54%, accroding to the theory a free dielectric water droplet should have expanded about 15%. A possbile explanation of this large difference is the surface underneath the sessile droplet. The surface provided the droplet with support and removed the need for axial symmetry. In other words there were fewer restraints on the droplet shape and therefore it was easier for the droplet to expand.

The ratios between the semi axis obtained from the free droplet theory was lower then the break up limit value of 1.9. Hence free droplets exposed to the fields used in this thesis work were expected to remain hole. In order for the free droplet break up criteria, eq (2.17), to be reached the voltage would have to be raised to 19 kV. Based on the findings of T.Schütte and S.

Hornfeldt it can be assumed that the same would apply to the sessile water drops. The sessile drops used in this experiment did not dissolve in any of the experiments conducted. That meant the breakup field strength was not reached. Since the highest voltage used during the experiments was 16 kV the experiments agree well with the theory.

5.5 Liquid-Contaminant Inclined-Plane Tracking and Erosion test

There was no significant difference in the surface roughness after one week of testing at 6 kV. After to weeks with the voltage set two 10 kV the surface appeared to be a little rougher, but not to a degree that could be called erosion of the surface, see figure 4.24. In order to obtain a definite answer to this erosion test, the test should have been conducted for a longer time period. In the test with the oil saturated sample, a much clearer erosion was discovered, see figure 5.3.

Even though the oil saturated sample was exposed to high voltage for a much shorter time, it had a much clearer erosion of the surface. This was in agreement with the data observed in the partial discharge test, where clearer and stronger partial discharges were observed for oil saturated samples.

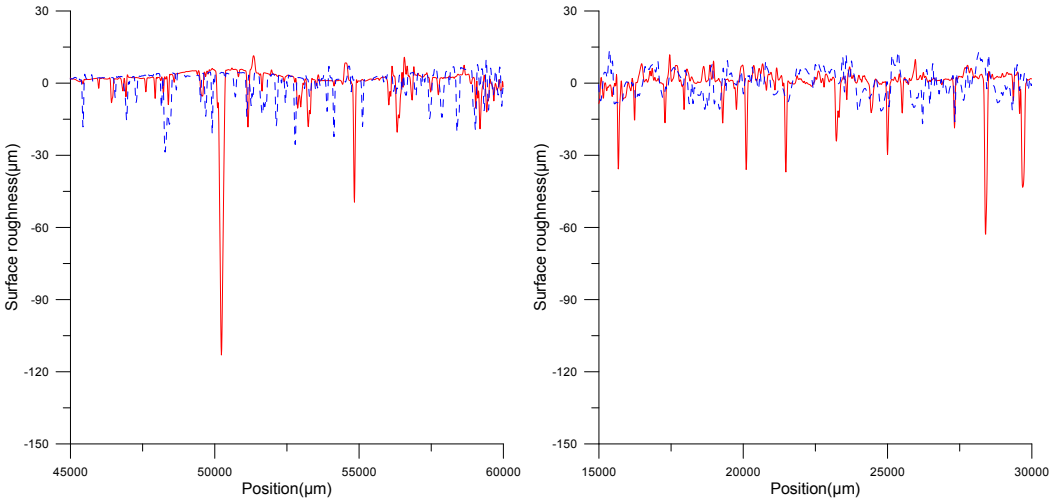

(a) Oil saturated sample

(b) Dry sample

Figure 5.3: Surface roughness around one of the dripping lines over the high voltage electrode. The red lines show the surface roughness after the voltage had been applied. The blue lines show the surface roughness before the voltage was applied.

Chapter 6

Conclusion

The presence of oil inside the sample had a huge effect on the droplet behavior. Expansion of droplet width occurred at lower voltage and was larger. Because of this partial discharges started at lower voltages, were stronger and more frequent. When the drops where made of salt water instead of deionized water the effects were even larger. This agrees well with the findings of Danikas et al, that greater droplet conductivity meant lower inception voltage [14]. The effects of oil inside the sample were larger than both the effect of placing droplets closer together and changing the volume of the droplets. The effect of increased droplet conductivity was the smallest of all the parameters varied.

The effects of oil on the discharges in the system were also visible in the erosion and tracking tests. When the sample was saturated with oil the erosion was more distinct and developed faster. When the insulation material was saturated with oil partial discharges were observed at voltage levels similar to those expected in the turbine. A system with a large probability of surface discharges will age faster. Based on this it appears that the oil component of the insulation system should be removed, in order to decrease the probability of discharges.

Future work

The reason for the large effect oil had on the inception voltage of the partial discharges for this insulating system were not discovered here. In order to obtain a good understanding of this situation more experimentation is necessary. Of the two hypothesis presented in this work, the most likely explanation is the change in friction between the droplet and surface. The information and experience obtained in this thesis work has provided a solid foundation for further experimentation. A good mold for construction of samples has been designed and many material properties investigated.

From an industrial point of view a longer and more detailed aging study should be conducted. In order to obtain better results these studies should be conducted on a larger scale, preferably on an actual turbine insulation system. This study has assumed that the oil is free to diffuse into the insulation system. Studies should be conducted in order to determine to what degree diffusion of oil into the insulation material is likely to occur.

Bibliography

[1] Bernt M. Grieg. Effects of moisture and oil on the dielectric properties of a glass fiber enforced epoxy composite. Projectwork, 2010.

[2] Dipl.-Ing. Sabine Keim. *Optical Diagnostic of Single Droplets on Polymeric Insulating Surfaces in an Electric Field. A Contribution to the Characterization of Phenomena Initiating Aging Mechanisms*. PhD thesis, Darmstadt University, 2003.

[3] G. Berg, L.E. Lundgaard, M. Becidan, and R.S. Sigrond. Instability of electrically stressed water droplets in oil, dielectric liquids. *Proceedings of 2002 IEEE 14th International Conference on Dielectric Liquids*, 2002.

[4] G.I. Taylor. Disintegration of water droplets in an electric field. *Proc. R. Soc. Lond., A 146, pp. 383-397*, 1964.

[5] A. Moukengué Imano and A. Beroual. Deformation of water droplets on solid surface in electric field. *Journal of Colloid and Interface Science Volume 298, Issue 2, 15 June 2006, Pages 869-879*, 2006.

[6] P.-G. de Gennes. Wetting: statics and dynamics. *Rev. Mod. Phys. 57, 827*, 1985.

[7] S. Keim, D. Koenig, and V. Hinrichsen. Experimental investigations on electrohydropdynamic phenomena at single droplets on insulating surfaces. *Annual report conference on Electrical Insulating and Dielectric Phenomena*, 2003.

[8] E. Kuffel, W.S. Zaengl, and J. Kuffel. *High Voltage Engineering: Fundamentals*, pages 433–440. Butterworth-Heinemann, 2000.

[9] Lars Lundgaard. Partielle utladninger - begreper, måleteknikk og mulige andvendelser for tilstandskontroll. Technical report, SINTEF Energiforskning, 1996.

[10] S. Feier-Iova and V. Hinrichsen. Partial discharge inception voltage of water drops on insulating surfaces stressed by electrical field. *Electrical Insulation Conference, 2009. EIC 2009. IEEE*, 2009.

[11] F. H. Kreuger. *Industrial High Voltage*, pages 117–132. Delf, The Netherlands: Delf Univerity Press, 1992.

[12] Knut Herstad and Walter Hansen. Plastisolasjon for offshore anlegg krypespor- og erosjonsprøver. Technical report, SINTEF, 1985.

[13] Ion I. Inculet, J.M.Floryan, and Ross Jeffrey Haywood. Dynamics of water drops breakup in electric fields. *IEEE Transactions on Industry Applications, Vol. 28, No. 5, Sept./Oct. 1992*, 1992.

[14] Michael G. Danikas, Ramanujam Sarathi, Pavlos Ramnalis, and Stefanos L.Nalmpantis. Analysis of polymer surface modifications due to discharges initiated by water droplets under high electric fields. *World Academy of Science, Engineering and Technology 50*, 2009.

[15] ASTM international. *Standard Test Mehods for Liquid-Contaminant Inclined-Plane Tracking and Erosion*, 2004.

[16] Mitutoyo Corporation. *Mitutoyo Surftest SV-2100 Surface Roughness Measuring system SV-2100 Series User' manual*, 2006.

[17] Ivan J.S.Lopes, Shesha H. Jayaram, and Edward A. Cherney. A study of partial discharges from water droplets on a silicone rubber insulationg surface. *IEEE Transactions on Dielectrics and Electrical Insulation*, 2001.

[18] Prathap Basappa, Vishnu Lakdawala, Bhargavi Sarang, and Ashtosh Mishra. Simulation of electric field distribution around water droplets on outdoor insulator surfaces. *Conference Record of the 2008 IEEE International Symposium on Electrical Insulation, 2008. ISEI 2008.*, 2008.

[19] L Lundgaard, G Berg, S Ingebrigtsen, and P Atten. *Emulsions and Emulsion Stability, 2nd ed. (edited by Johan Sjøblom)*, pages Chapter 15, pp. 549 – 592. Taylor and Francis, 2006.

[20] T.Schutte and S. Hornfeldt. Dynamics of electrically stressed water drops on insulating surfaces. *Conference Record of the 1990 IEEE International Symposium on Electrical Insulation, Toronto. Canada, June 3-6, 1990*, 1990.

Appendix A

This appendix shows how one salt water droplet changed under the influence of an electric field on an oil saturated sample.

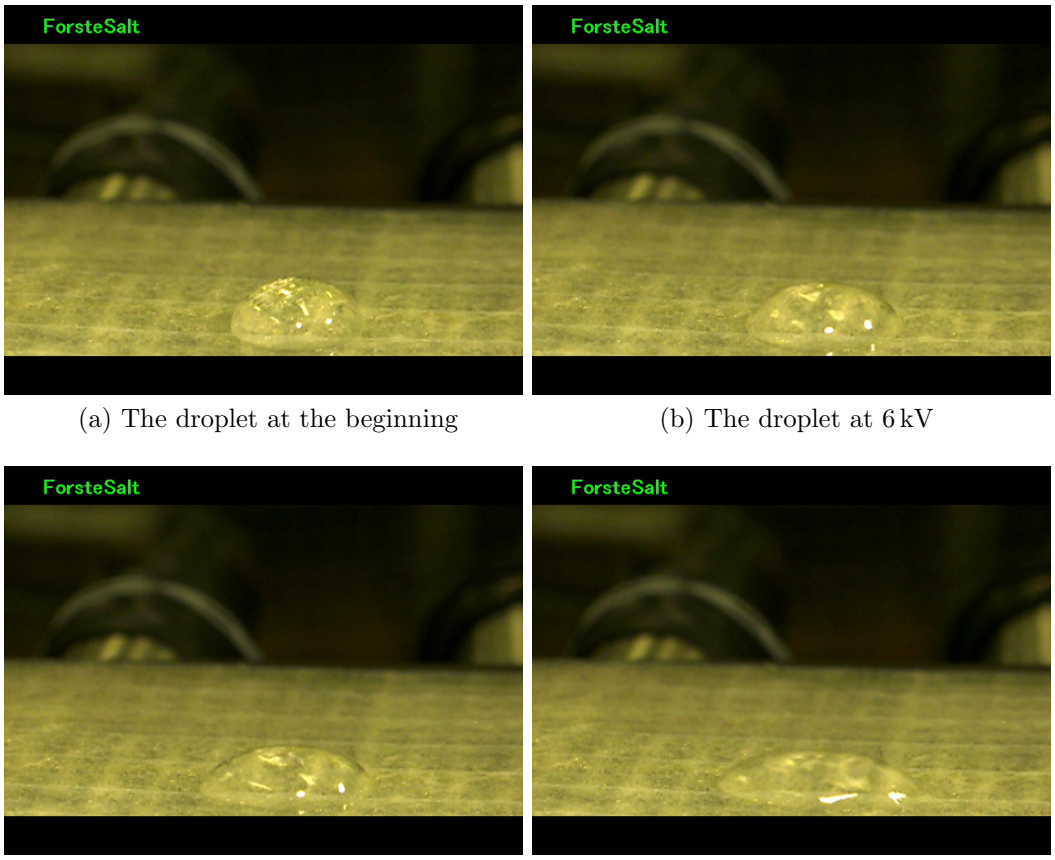

(a) The droplet at the beginning

(b) The droplet at 6 kV

(c) The droplet at 8 kV

(d) The droplet at 10 kV

Figure A.1: 100 µL salt water droplet in an electric field on an oil saturated surface.

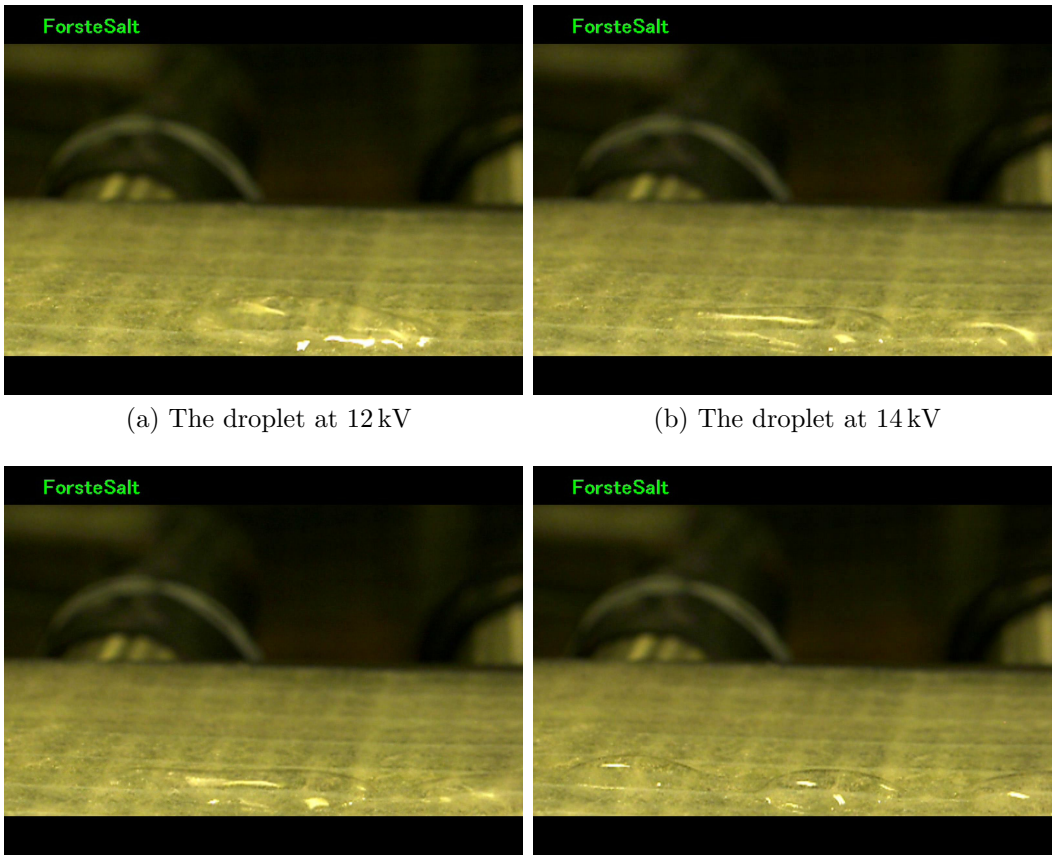

(a) The droplet at 12 kV

(b) The droplet at 14 kV

(c) The droplet at 16 kV

(d) The droplet at the end

Figure A.2: 100 µL salt water droplet in an electric field on an oil saturated surface.